Available online at www.sciencedirect.com
ScienceDirect
Chemistry and Physics of Lipids 148 (2007) 26–50
CPL
CHEMISTRY AND PHYSICS OF LIPIDS
www.elsevier.com/locate/chemphyslip

The thermotropic phase behaviour and phase structure of a homologous series of racemic β-D-galactosyl dialkylglycerols studied by differential scanning calorimetry and X-ray diffraction

David A. Mannock [a,*], Marcus D. Collins [b,1], Manfried Kreichbaum [c], Paul E. Harper [d], Sol.M. Gruner [b], Ronald N. McElhaney [a,*]

[a] *Department of Biochemistry, University of Alberta, Edmonton, Alta. T6G 2H7, Canada*
[b] *CHESS & Department of Physics, Cornell University, 162 Clark Hall, Ithaca, NY 14853-2501, USA*
[c] *Austrian Academy of Sciences, Institute of Biophysics and X-ray Structure Research, Schmiedlstrasse 6, A-8042 Graz, Austria*
[d] *Department of Physics and Astronomy, Calvin College, 3201 Burton St. SE, Grand Rapids, MI 49546, USA*

Received 10 January 2007; accepted 10 April 2007
Available online 19 April 2007

Abstract

The thermotropic phase behaviour of aqueous dispersions of some synthetic 1,2-di-*O*-alkyl-3-*O*-(β-D-galactosyl)-*rac*-glycerols (*rac*-β-D-GalDAGs) with both odd and even hydrocarbon chain lengths was studied by differential scanning calorimetry (DSC), small-angle (SAXS) and wide-angle (WAXS) X-ray diffraction. DSC heating curves show a complex pattern of lamellar (L) and nonlamellar (NL) phase polymorphism dependent on the sample's thermal history. On cooling from 95 °C and immediate reheating, *rac*-β-D-GalDAGs typically show a single, strongly energetic phase transition, corresponding to either a lamellar gel/liquid-crystalline (L_β/L_α) phase transition ($N \leq 15$ carbon atoms) or a lamellar gel/inverted hexagonal (L_β/H_{II}) phase transition ($N \geq 16$). At higher temperatures, some shorter chain compounds ($N = 10$–13) exhibit additional endothermic phase transitions, identified as L/NL phase transitions using SAXS/WAXS. The NL morphology and the number of associated intermediate transitions vary with hydrocarbon chain length. Typically, at temperatures just above the L_α phase boundary, a region of phase coexistence consisting of two inverted cubic (Q_{II}) phases are observed. The space group of the cubic phase seen on initial heating has not been determined; however, on further heating, this Q_{II} phase disappears, enabling the identification of the second Q_{II} phase as $Pn\bar{3}m$ (space group Q^{224}). Only the $Pn\bar{3}m$ phase is seen on cooling.

Under suitable annealing conditions, *rac*-β-D-GalDAGs rapidly form highly ordered lamellar-crystalline (L_c) phases at temperatures above ($N \leq 15$) or below ($N = 16$–18) the L_β/L_α phase transition temperature (T_m). In the $N \leq 15$ chain length lipids, DSC heating curves show two overlapping, highly energetic, endothermic peaks on heating above T_m; corresponding changes in the first-order spacings are observed by SAXS, accompanied by two different, complex patterns of reflections in the WAXS region. The WAXS data show that there is a difference in hydrocarbon chain packing, but no difference in bilayer dimensions or hydrocarbon chain tilt for these two L_c phases (termed L_{c1} and L_{c2}, respectively). Continued heating of suitably annealed, shorter chain *rac*-β-D-GalDAGs from the L_{c2} phase results in a phase transition to an L_α phase and, on further heating, to the same Q_{II} or H_{II} phases observed on first heating.

* Corresponding authors. Tel.: +1 780 492 2412/2413; fax: +1 780 492 0095.
E-mail addresses: dmannock@ualberta.ca (D.A. Mannock), rmcelhan@ualberta.ca (R.N. McElhaney).
[1] Present address: Department of Chemistry, University of Washington, Box 351700, Seattle, WA 98195-1700, United States.

doi:10.1016/j.chemphyslip.2007.04.004

On reheating annealed samples with longer chain lengths, a subgel phase is formed. This is characterized by a single, poorly energetic endotherm visible below the T_m. SAXS/WAXS identifies this event as an L_c/L_β phase transition. However, the WAXS reflections in the di-16:0 lipid do not entirely correspond to the reflections seen for either the L_{c1} or L_{c2} phases present in the shorter chain *rac*-β-D-GalDAGs; rather these consist of a combination of L_{c1}, L_{c2} and L_β reflections, consistent with DSC data where all three phase transitions occur within a span of 5 °C. At very long chain lengths ($N \geq 19$), the L_β/L_c conversion process is so slow that no L_c phases are formed over the time scale of our experiments. The L_β/L_c phase conversion process is significantly faster than that seen in the corresponding *rac*-β-D-GlcDAGs, but is slower than in the 1,2-*sn*-β-D-GalDAGs already studied. The L_α/NL phase transition temperatures are also higher in the *rac*-β-D-GalDAGs than in the corresponding *rac*-β-D-GlcDAGs, suggesting that the orientation of the hydroxyl at position 4 and the chirality of the glycerol molecule in the lipid/water interface influence both the L_c and NL phase properties of these lipids, probably by controlling the relative positions of hydrogen bond donors and acceptors in the polar region of the membrane.

Keywords: Galactolipids; Lipid polymorphism; Lipid thermotropic phase behaviour; Inverted hexagonal phase; Inverted cubic phase; Differential scanning calorimetry; X-ray diffraction

1. Introduction

There is great interest in the physical properties of the monoglycosyl diglycerides (MGDGs) in which a single carbohydrate, usually a hexopyranoside, is attached via an α or β linkage to either a diacyl or dialkyl glycerol (Fig. 1). For many years, the diacyl glycoglycerolipids were mostly thought to be important as structural elements in the membranes of a wide variety of photosynthetic plants and microorganisms (Williams and Quinn, 1987; Fischer, 1990; Smith, 1988; Brennan, 1988; Ishizuka and Yamakawa, 1985), where they are required for the proper functioning of the photosynthetic reaction centre (Williams and Quinn, 1987; Camara-Artigas et al., 2002; Pick et al., 1987; Hagio et al., 2000; Sato et al., 1995, 2003; Minoda et al., 2002; Benning, 1998; Yu et al., 2002) and for the maintenance of chloroplast morphology (Hartel et al., 1998). However, recent advances in medical research have shown that some glycolipids containing a single sugar unit may have several coexisting functions in cell membranes, which may combine regulatory, immunological and structural roles. Specific occasions on which this multifunctional role has been identified in glycolipids include a role in regulating triggered cell death by α-D-galactosylceramide (Nicol et al., 2000; Saubermann et al., 2000; Kitamura et al., 2000) and other glycolipids (Zhao et al., 1999), and the role of the seminolipid (1-*O*-hexadecyl-2-*O*-hexadecanoyl-3-*O*-β-D-(3′-sulfo)-galactopyranosyl-*sn*-glycerol; 3′-SO_3-β-D-GalAAG) in the formation of the myelin sheath and in spermatogenesis (Honke et al., 2002). The seminolipid is also intimately involved in the events leading to fertilization, which involves both the binding of the sperm to the ovum *zona pellucida* (White et al., 2000), as well as a change in the ratio of lamellar- and nonlamellar-preferring lipids following removal of the sulfate group by the extracellular arylsulfatase A, which may promote the fusion of the spermatozoa membrane with that of the ovum (Gadella et al., 1995). The 3′-SO_3-β-D-GalAAG is also responsible for the binding and transfection of certain species of *Mycoplasma* that are known to cause infertility in humans (Lingwood et al., 1990; Tsuji et al., 1992), as well as the binding of viruses such as influenza virus type A (Nakata et al., 2000) and the human immunodeficiency virus causing AIDS (Brogi et al., 1998; Lau et al., 1993; Loya et al., 1998; Mizushina et al., 2003; Murakami et al., 2003; Mannock and McElhaney, 2004, and references therein). Also, 3′-SO_3-β-D-GalAAG may be responsible for the binding of the HIV glycoprotein 120 to spermatozoa and subsequent transmission of HIV to the sexual partner (Brogi et al., 1998 and references therein).

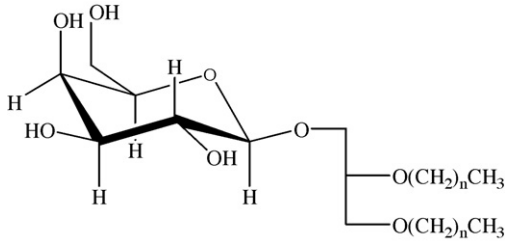

Fig. 1. The chemical structure of the racemic dialkyl-β-D-galactosyl glycerols used in this study.

Studies of the plant glycolipids have shown that both the nonionic galactolipids and the sulfonoquinovosyldiacylglycerol are potent inhibitors of both eukaryotic DNA polymerases and the HIV reverse transcriptase (Lau et al., 1993; Loya et al., 1998; Mizushina et al., 2003; Murakami et al., 2003; Mannock and McElhaney, 2004, and references therein). In addition, both ionic and nonionic glycolipids have been shown to be potent inhibitors of tumour growth in a variety of cancers (Lu

et al., 1994; Colombo et al., 2002; Sahara et al., 2002; Ohta et al., 2001; Mannock and McElhaney, 2004, and references therein). Thus, MGDGs are of importance as both immunological and regulatory elements in the native membranes in which they are found and for their pharmacological properties. They are presently being investigated for use in a variety of biomedical applications (Mannock and McElhaney, 2004, and references therein).

Prior to 1985, physical studies of the glycoglycerolipids were confined to a few studies of native diacyl-β-D-galactosyl-*sn*-glycerols isolated from photosynthetic organelles (Rivas and Luzzati, 1969; Shipley et al., 1973; Oldani et al., 1975; Mannock et al., 1985b; Sanderson and Williams, 1992), their hydrogenated derivatives (Sen et al., 1983; Mannock et al., 1985a; Quinn and Lis, 1987; Lis and Quinn, 1986) and the corresponding α-D-glucolipids isolated from *Acholeplasma laidlawii* (Wieslander et al., 1978, 1981a,b; Khan et al., 1981; Silvius et al., 1980). More recently, the synthesis of the 1,2-diacyl-α- and β-D-glucosyl- and β-D-galactosyl-*sn*-glycerols and their subsequent physical studies (Mannock et al., 2001a,b; Yue et al., 2003; Asgharian et al., 2000; Lewis et al., 1997, and references therein) have demonstrated the existence of a rich pattern of lamellar and nonlamellar polymorphism in aqueous dispersions of the above glycolipids, together with a more complex structural regulation of lipid membrane architecture than had hither to been envisaged (Lewis et al., 1997; Mannock and McElhaney, 2004, and references therein).

In contrast, the corresponding dialkyl glycolipids have been isolated from fewer sources, most of which are halotolerant or methanogenic archaebacteria (Fischer, 1990). The chirality of the glycerol backbone in these native glycosyl dialkylglycerols is exclusively 2,3-*sn*, whereas that of their diacyl counterparts from bacterial and eucaryotic cells is exclusively 1,2-*sn* (Fischer, 1990). This raises the question of whether there is any biological significance in such differences in glycerol configuration and what, if any, role they might play in regulating the lateral compressibility and interfacial curvature of the resulting membranes.

The presence of a second chiral centre in the sugar portion of the glycolipid molecule (D- or L-galactose) makes studies of any one representative lipid chemical configuration more complicated, because two lipids containing identical sugar headgroups (D-galactose), but glycerols of opposite chirality, are not enantiomers, but diastereomers. There have been several recent studies which show that phospholipids differing in their chirality in the headgroup and interfacial regions may also have different physical properties (Wisner et al., 1986; Brain et al., 1986; Silvius et al., 1986; Bruzik and Tsai, 1987). This has prompted us to ask whether the recent reports of the thermotropic properties of a small number of 1,2-dialkyl-3-*O*-(β-D-glucosyl)- and (β-D-galactosyl)-*sn*-glycerols are also representative of the natural 2,3-*sn* diastereomers, as has been implied (Hinz et al., 1991; Jarrell et al., 1987; Kuttenreich et al., 1988, 1993; Mannock et al., 1992, 1994, and references therein). In order to investigate this possibility further, we have utilized established procedures (Ogawa and Beppu, 1982; Mannock et al., 2000) to facilitate the synthesis of a series of compounds in which the configuration of both the carbohydrate headgroup and dialkyl glycerol can be systematically varied. In this paper, we describe the thermotropic phase behaviour of a series of synthetic dialkyl-β-D-galactosyl-*rac*-glycerols (*rac*-β-D-GalDAGs), with alkyl chain lengths ranging from 10 to 20 carbon atoms, using differential scanning calorimetry (DSC) and small-angle (SAXS) and wide-angle (WAXS) X-ray diffraction.

2. Materials and methods

2.1. Synthesis

Racemic dialkyl glycerols were prepared according to the procedure of Mangold and co-workers (Baumann and Mangold, 1966a,b). All other materials were prepared as reported earlier (Baumann and Mangold, 1966a; Mannock et al., 1987; Mannock and McElhaney, 1991). The methodology used for the preparation of an extensive range of *rac*-β-D-GalDAGs with different chain lengths are the same as those reported for the corresponding *rac*-β-D-glucosylDAGs (Mannock et al., 2000). This glycosylation reaction was high yielding (70–80%) and successful in all cases, producing anomeric ratios varying from 4:1 to 8:1 (β:α), depending on the chain length. The individual anomers were then separated by column chromatography. A full description of the methodology and purification processes used for the preparation of these *rac*-β-D-GalDAGs have been reported for the corresponding β-D-glucosyl compounds (Mannock et al., 2000), which utilized the same batch of synthetic dialkyl-*rac*-glycerols. The chemical structure of the *rac*-β-D-GalDAGs is shown in Fig. 1. All analytical measurements were consistent with the assigned structures and were in agreement with literature values and indicated a purity of ≥97% with an anomeric ratio of 20:1 (β/α) or better.

2.2. Physical measurements

Low-sensitivity DSC measurements were performed using a Perkin-Elmer DSC-2C (PE-DSC) equipped with a 3600 series Thermal Analysis Data Station using TADS software. Lipid samples were prepared by weighing the freeze-dried lipid into a stainless steel capsule using a Fisher/Mettler M3 microgramatic balance, whereupon 50 μL de-ionized water was added. The capsule was then sealed and placed into the DSC sample cell, while a similar capsule containing de-ionized water was placed in the reference cell. Both were then cycled between 5 and 90 °C at a rate of 20 °C/min to ensure that the lipid was fully hydrated, as determined by the repeatability of heating and cooling scans. Data was subsequently collected over the range of 5–95 °C at heating and cooling rates varying from 20 to 0.3 °C/min. Data files were transformed into an ASCI file format for further analysis and were imported into Origin 7.5 (Originlab Corp., Northampton, MA).

High-sensitivity DSC measurements were performed using a Calorimetry Sciences Corporation Multicell-DSC (CSC-DSC; American Fork, UT, USA). The samples were prepared by weighing the dry lipid into the cell using a Fisher/Mettler M3 microgramatic balance; 0.5 mL de-ionized water was added and the cell was sonicated in a water bath for 20 min at room temperature. The cells were then manually dried and placed into the CSC-DSC, whereupon they were cycled between 10 and 90 °C at 30 °C/h to ensure uniform mixing of the sample prior to storage at 4 °C for 24 h and followed by measurement. Data was collected over the range of 5–95 °C at a rate of 10 °C/h and was imported into Origin 7.5 (Originlab Corp., Northampton, MA) for further analysis.

Samples were prepared for X-ray diffraction (XRD) by first placing 3–5 mg of dry lipid into a 1.5 mm glass X-ray capillary sealed with either a flame or 5-min epoxy at the small end, followed by the addition of 7–10 μL deionized water. The lipids typically floated if the mixture was centrifuged, so the mixture was first mixed mechanically. After flame sealing the open end, the contents of the capillary were further mixed by repeated centrifugation in a table-top centrifuge, flipping the capillary 180° between each centrifugation. Samples were then transferred to an X-ray camera stage fitted with a Peltier-controlled thermostat (±0.5 °C). In most cases, the sample was slowly heated from 10 °C to 90 or 95 °C and brought back to 10 °C over the course of 12–18 h to anneal and improve mixing. The samples were determined to be uniformally dispersed when different parts of the X-ray capillary all yielded the same diffraction.

Two X-ray diffraction systems were used to collect data: the first was attached to a Rigaku RU200 rotating anode generator (MSC-Rigaku, The Woodlands, TX) with a copper anode producing Cu Kα X-rays with a wavelength of 1.54 Å and consisted of crossed Franks mirrors equipped with a slow scan SIT-TV detector (Gruner et al., 1982; Shyamsunder et al., 1988). The second system, which was used to collect both SAXS and WAXS diffraction patterns, consisted of a Rigaku RU300 rotating anode generator also producing Cu Kα X-rays which were doubly focused using two perpendicular Franks mirrors. The diffracted images were then collected using an image intensified, fibre optically coupled CCD camera (Tate et al., 1997) and were then digitally transferred to a computer. In both cases, the sample temperature was regulated by means of a sample holder whose temperature was computer-controlled by thermoelectrics to ±0.5 °C.

Following the first thermal cycle described above, samples were incubated overnight at 10 °C. The XRD measurements were performed on each lipid sample over the range −20 to 90 °C in both the heating and cooling directions at intervals of 5 or 10 °C. Samples were allowed to equilibrate for 30–60 min after each temperature change before collecting new diffraction images. Both SAXS and WAXS scattering data were collected for selected lipid chain lengths. The SAXS and WAXS procedures differ only in the distance from the specimen to the detector. Generally, the diffraction patterns showed only two to four powder reflections, although as many as seven orders were visible for some samples. Lattice parameters (a) determined by SAXS were accurate to ±0.05 nm, whereas the WAXS spacings were accurate to ±0.01 nm. The reflections in the small-angle region were used to identify the phase morphology, whereas the wide-angle spacings provided details of the hydrocarbon chain packing (Fig. 2).

3. Results

3.1. Calorimetric measurements

Heating and cooling thermograms of a homologous series of *rac*-β-D-GalDAGs containing alkyl chains with odd and even numbers of carbon atoms, obtained using the PE-DSC-2, are shown in Fig. 3. The corresponding thermodynamic parameters are listed in Table 1 and are plotted as a function of hydrocarbon chain length in Fig. 4.

Initial heating and cooling experiments over a wide range of temperature (5–95 °C) and scan rate (20–0.3 °C/min) using the PE-DSC2 showed that the

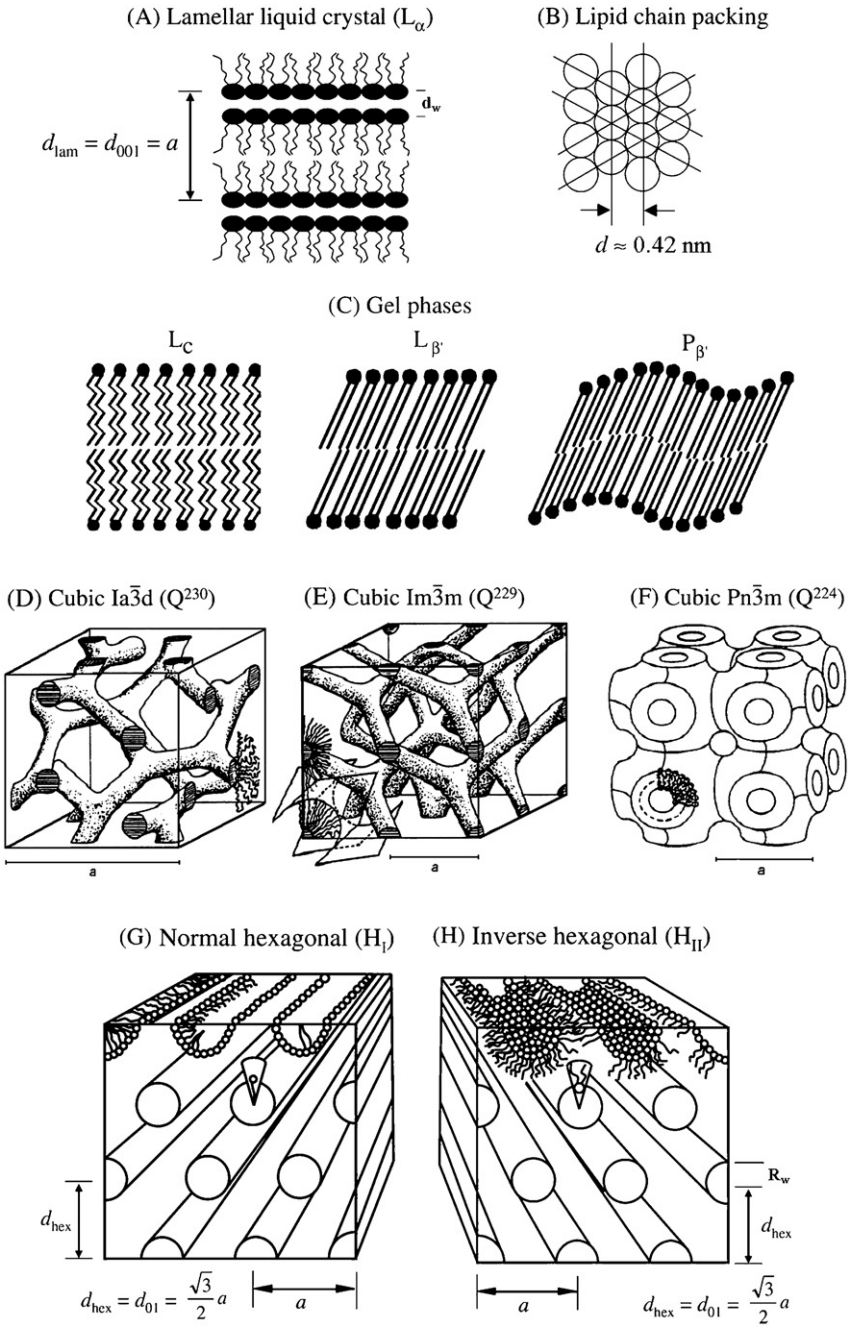

Fig. 2. A schematic drawing of various lipid-water mesophases and states of aggregation adopted by membrane lipids: (A) L_α, lamellar liquid-crystalline; (B) cross-sectional view of the acyl chains in a hexagonal close-packed arrangement (the view is along the chain axis); (C) various gel phases (L_c, lamellar crystalline; $L_{\beta'}$, lamellar gel phase with tilted chains; $P_{\beta'}$, ripple gel phase); (D)–(F) $Ia\bar{3}d$ (Q^{230}, Q_{II}^G), $Im\bar{3}m$ (Q^{229}, Q_{II}^P), $Pn\bar{3}m$ (Q^{224}, Q_{II}^D) inverse bicontinuous cubic phases. The cubic phases are represented by the G, P and D minimal surfaces, which locate the midplanes of fluid lipid bilayers; (G) H_I normal and (H) H_{II} inverted hexagonal phase. After Gabke et al. (2005) and Seddon et al. (2000).

pattern of mesophase behaviour in the shorter chain compounds ($n = 10{:}0$–$14{:}0$) was complicated by the rapid formation of one or more L_c phases. The rate of L_c phase formation from the L_β phase (which also exhibited odd–even alternation) was so rapid that it was not possible to isolate the L_β phase in pure form in those compounds using these standard protocols (data not shown). In order to isolate the mesophases in these lipids,

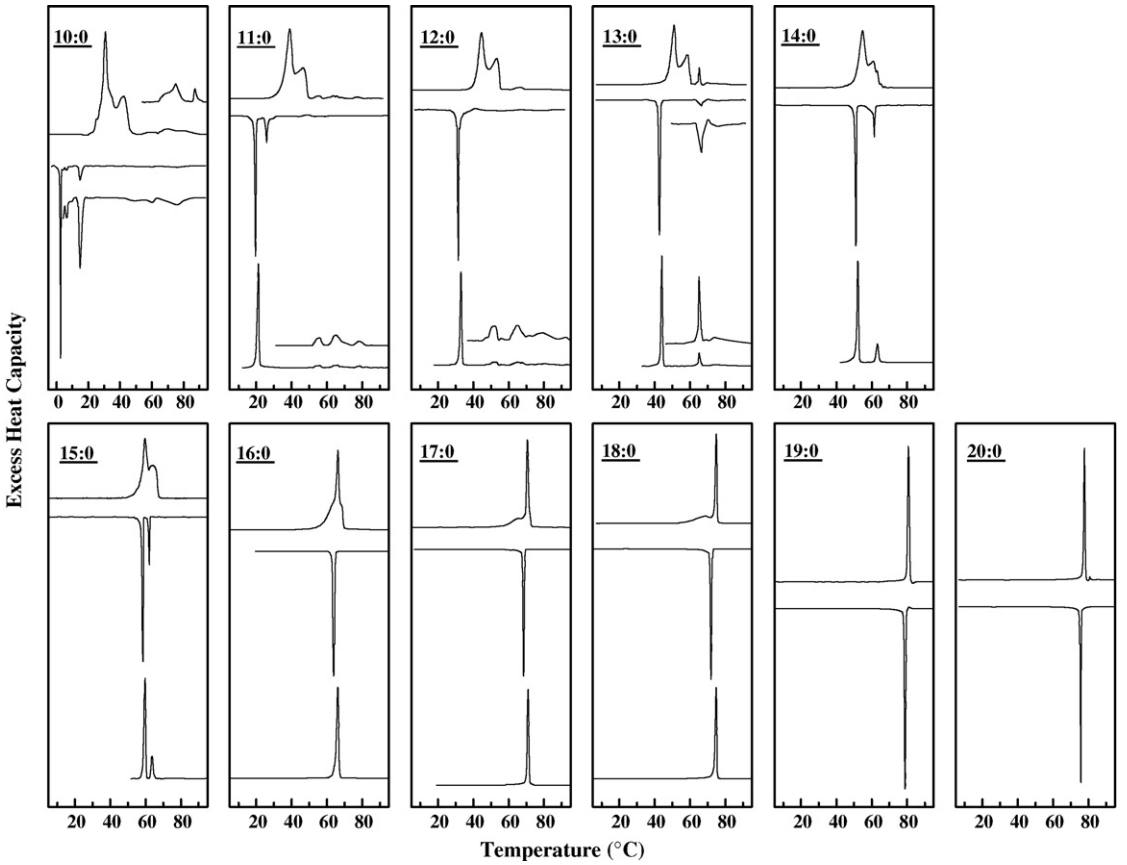

Fig. 3. Low-sensitivity DSC thermograms of a series of synthetic racemic dialkyl-β-D-galactosyl-glycerols with hydrocarbon chain lengths ranging from 10 to 20 carbon atoms. The heating and cooling rates are 1 °C/min, unless specified otherwise. In each panel, the sequence of thermograms is as follows: the upper scan is the first heating scan of the annealed lipid samples in the L_c phase, except for the lipids with 19 and 20 carbon chain lengths where no L_c phase was observed; the middle scan is a cooling scan; and the lowest scan is the second heating scan from the L_β phase, except for the di-10:0 lipid where the rapid L_β/L_c phase conversion did not permit its isolation. The y-axis expansions are situated above the second heating scans and, in the di-10:0 lipid, below the cooling scan.

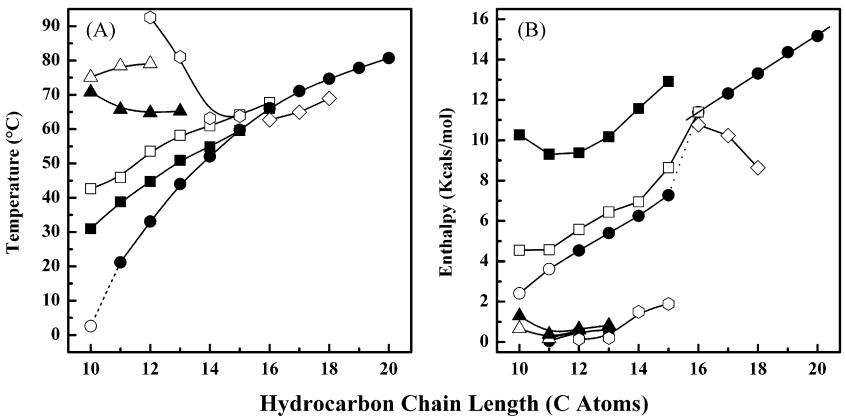

Fig. 4. Measurements of (A) the phase transition temperatures (T, °C) and (B) the enthalpies (ΔH, kcal/mol) calculated from heating scans obtained from the PE-DSC2 of a homologous series of racemic dialkyl-β-D-galactosyl-glycerols as a function of chain length. Symbols: (■) L_{c1}/X; (□) L_{c2}/X; (●) $L_\beta/L_\alpha \leq 15$ and $L_\beta/H_{II} \geq 16$; (○) L_α/L_β; (▲) L_α/Q^a_{II}; (△) Q^a_{II}/Q^{224}; (⬡) L_α/H_{II}; (◇) L_c/L_β.

Table 1
Phase transition properties of a series of synthetic 1,2-di-*O*-alkyl-3-*O*-(β-D-galactopyranosyl)-*rac*-glycerols obtained from heating scans using the PE-DSC2

Chain length	Phase transition															
	L_β/L_α		L_β/H_{II}		L_α/Q_{II}		Q_{II}/Q_{II}		Q_{II}/H_{II}		L_α/H_{II}		$L_{c1}/?$[a]		$L_{c2}/?$[a]	
	T_m	ΔH	T_m	ΔH	T_{NL}	ΔH	T_{NL}	ΔH	T_h	ΔH	T_h	ΔH	T_x	ΔH	T_x	ΔH
10:0	*2.4*	*1.8*		–	64.8	1.3	75.1	0.7					30.9	10.3	42.6	4.5
11:0	21.2	2.8		–	62.3	0.4	77.8	0.2					38.8	9.3	45.9	4.6
12:0	33.1	3.4		–	62.5	0.6	79.1	0.6	92.5[c]	0.14			44.7	9.9	53.6	5.8
13:0	44.0	4.9		–	63.2	0.8	∼81[b]	–	∼81[b]	0.2[b]			50.9	7.7	58.1	6.4
14:0	52.1	6.3		–	–	–	–	–	–	–	63.2	1.5	54.9	11.6	60.9	6.9
15:0	59.8	7.3		–	–	–	–	–	–	–	63.8	1.9	59.6	12.9	64.2	8.6
16:0	–	–	65.8	11.4	–	–	–	–	–	–			62.7	10.8	67.7	11.4
17:0	–	–	70.6	12.3	–	–	–	–	–	–			64.9	10.2		
18:0	–	–	74.3	13.3	–	–	–	–	–	–			68.9	8.6		
19:0	–	–	78.1	14.4	–	–	–	–	–	–				–		
20:0	–	–	81.4	15.2	–	–	–	–	–	–				–		

Transition temperatures (T_x) are cited in degrees Celsius and transition enthalpies (ΔH) are given in kcal/mol. Values in italics are from the corresponding cooling experiment where it was not possible to perform an accurate measurement in the heating direction.

[a] The nature of the transitions from these L_c phases changes with chain length, see Fig. 4 and the text for details.

[b] We could not accurately separate the exo- and endothermic components of the Q_{II}/H_{II} phase transition seen in the di-13:0 lipid.

[c] Initially the transition to the H_{II} phase was observed at a temperature of 102 °C.

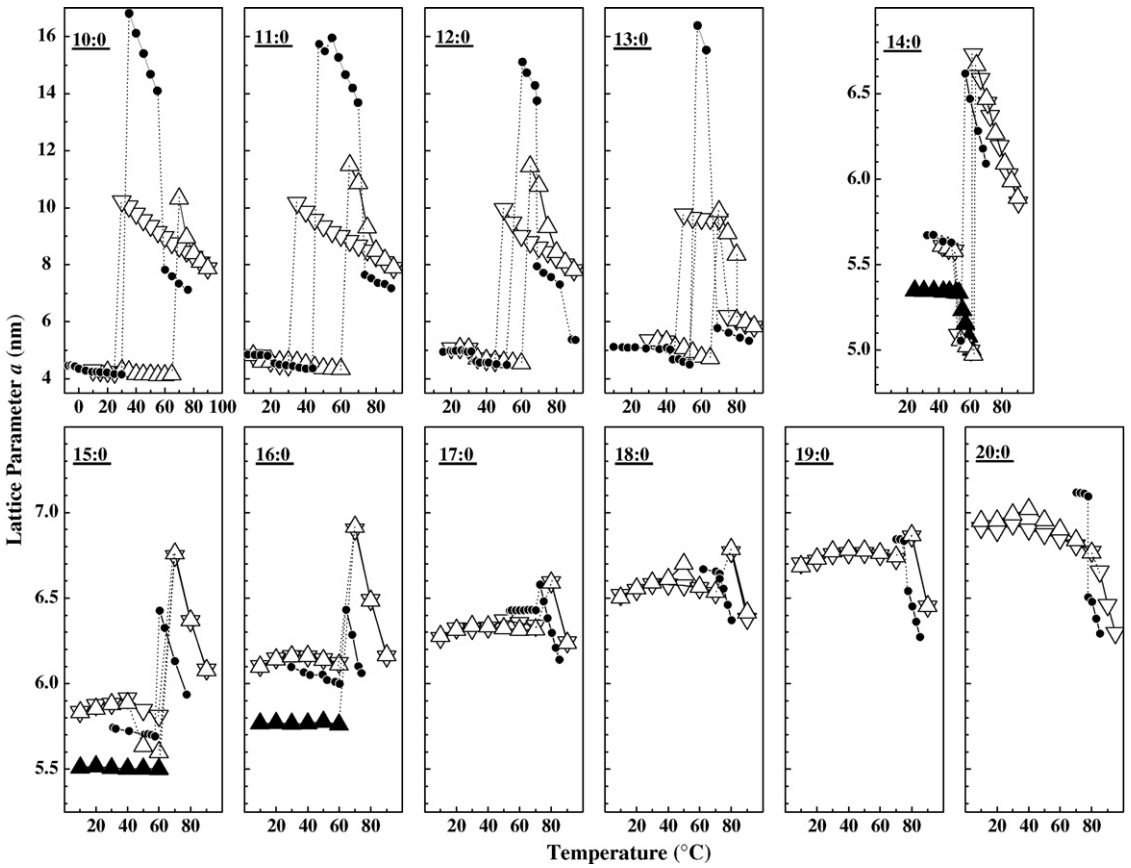

Fig. 5. Small-angle X-ray diffraction measurements of the racemic dialkyl-β-D-galactosyl- and β-D-glucosyl-glycerols, showing plots of the cell lattice parameter (a, nm) as a function of temperature (°C). Symbols: (△) heating direction; (▽) cooling direction; (▲) heating from the L_c phase; (●) heating measurements of the corresponding glucolipids (Mannock et al., 2000).

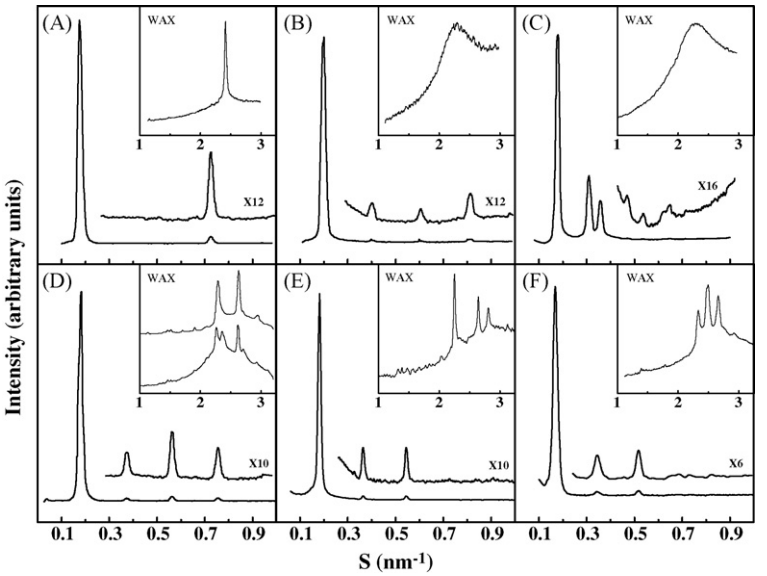

Fig. 6. SAXS and WAXS (inset) patterns for samples of the racemic dialkyl-β-D-galactosyl-glycerols with representative hydrocarbon chain lengths. (A) 14:0 L_β phase at 20 °C. (B) L_α phase at 55 °C. (C) H_{II} phase at 65 °C. (D) L_{c1} phase at 20 °C. In the inset, the upper WAXS pattern is the L_{c1}, whereas the lower pattern is the L_{c2} phase at 58 °C. (E) 15:0 L_{c1} phase at 1 °C. (F) 16:0 $L_{c1}/L_{c2}/L_\beta$ phase mixture at 1 °C. The SAXS and WAXS spacings are listed in Tables 2 and 3 together with calculations derived from those spacings.

the samples were cooled from 95 °C at a rate of 1 °C/min to just below their respective L_β/L_α phase transition temperatures and immediately reheated. Under such conditions, a single sharp, highly energetic phase transition was observed at lower temperatures, which SAXS and WAXS (Figs. 5 and 6; Tables 2 and 3) confirmed as the L_β/L_α phase transition.

It was necessary to apply this experimental protocol in both the DSC and XRD measurements in order to isolate the metastable L_β phase in all lipid samples between chain lengths of 11–15 carbon atoms. We were unable to isolate the L_β phase in the heating direction of the *rac*-di-10:0-β-D-GalDAG using the PE-DSC (Fig. 3) and of both the *rac*-di-10:0- and di-11:0-β-D-GalDAGs using the CSC-DSC. This was despite the fact that exothermic peaks, corresponding to the L_α/L_β phase transition, were evident in the cooling scans, suggesting that the L_c phase might be formed from a transient L_β phase on cooling at shorter chain lengths. With increasing chain length as the L_β/L_c conversion rate decreases, the chain-melting phase transition becomes visible in the heating direction and is reversible on cooling. The nature of this phase transition changes with increasing chain length. At shorter chain lengths (11:0–15:0), SAXS/WAXS measurements confirm the existence of an L_β/L_α phase transition, whereas longer chain length samples (16:0–20:0) exhibit an L_β/H_{II} phase transition (see below).

At temperatures above the L_β/L_α phase transition in the shorter chain *rac*-β-D-GalDAGs ($N \leq 15$), one or more poorly energetic thermal events are visible in the CSC-DSC heating thermograms, which vary in their transition temperature, enthalpy (ΔH) and peak width according to the length of the hydrocarbon chains. In samples of the *rac*-di-10:0- to di-13:0-β-D-GalDAGs, a single phase transition is visible at 62–64 °C, corresponding to a lamellar liquid crystalline to an inverted cubic (L_α/Q^a_{II}) phase transition as seen by SAXS measurements. In the case of the *rac*-di-11:0- to di-13:0-β-D-GalDAGs, there was some evidence of a combination of an endotherm immediately followed by an exothermic event at this temperature in the CSC-DSC heating thermograms, suggesting a complex process whose nature remains undetermined. Both the PE-DSC and the CSC-DSC show the existence of these phase transitions at about 62 °C.

Samples of *rac*-di-11:0 and di-12:0-β-D-GalDAGs measured in the PE-DSC also show a single thermal event below 62 °C, but there is no evidence of a similar peak in the di-10:0 or 13:0 lipid. There are also no peaks at corresponding temperatures in the heating thermograms of annealed samples of those lipids, eliminating the possibility of the formation of L_c phases during the heating scan. The likelihood that the poorly energetic peaks below 62 °C are the result of some kinetic artifact cannot be ruled out, as they do not appear in the

Table 2
X-ray diffraction *d*-spacings (nm) at specified temperatures (°C) and dimensional thermal expansion coefficients (s, nm/K) for the L_c, L_β, L_α, Q_{II} and H_{II} phases of (A) the 1,2-di-*O*-alkyl-3-*O*-β-D-galactopyranosyl-*rac*-glycerols and (B) the 1,2-di-*O*-alkyl-3-*O*-β-D-glucopyranosyl-*rac*-glycerols (Mannock et al., 2000) dispersed in water, as a function of chain length (number of carbon atoms)

CL	Phase	(A) d[a] (nm)	T (°C)	$s^T \times 10^{-3}$ (nm/K)	(B) d[a] (nm)	T (°C)	$s^T \times 10^{-3}$ (nm/K)
10:0	L_{c1}	4.30	30	–[b]	*na*	*na*	*na*
	L_{c2}	4.24	35	–[b]	*na*	*na*	*na*
	L_β	–	–	–	4.42	−2	−3.46
	L_α	4.15	40	−1.20	4.15	30	−6.00
	Q_{II}[c]	7.30 (**10.32**)[d]	70	−276.0	6.86 (**16.80**)[e]	35	−138.5
		5.95 (**8.35**)[f]	80	−38.65	5.52 (**7.81**)[f]	60	−44.30
11:0	L_{c1}	4.60	30	−0.4	*na*	*na*	*na*
	L_{c2}	4.42	45	−1.70	*na*	*na*	*na*
	L_β	4.82	10	–[b]	4.83	11	−3.11
	L_α	4.36	50	−3.00	4.54	22	−9.01
	Q_{II}[c,g]	8.13 (**11.49**)[d]	65	−211.2	6.51 (**15.96**)[e]	55	−150.1
		6.00 (**8.49**)[f]	80	−38.06	5.40 (**7.64**)[f]	73	−46.6
12:0	L_{c1}	–	–	–	*na*	*na*	*na*
	L_{c2}	–	–	–	*na*	*na*	*na*
	L_β	5.06	30	−2.00[h]	4.96	31	0.13
	L_α	4.56	60	−6.80	4.61	33	−6.63
	Q_{II}[c,g]	8.10 (**11.45**)[d]	65	−209.4	6.17 (**15.1**)[e]	60	−143.8
		5.79 (**8.20**)[f]	80	−39.14	5.45 (**7.71**)[f]	73	−43.40
	H_{II}	–	–	–	4.62 (**5.33**)	88	–[b]
13:0	L_{c1}	5.11	45	−0.6	*na*	*na*	*na*
	L_{c2}	4.92	55	−32.00[b]	*na*	*na*	*na*
	L_β	5.31	40	−3.00[h]	5.05	40	−2.43
	L_α	4.76	60	−6.00	4.70	43	−1.75
	Q_{II}[c,g]	6.99 (**9.88**)[d]	70	−152.0	6.68 (**16.37**)[e]	58	−168.2
		6.88[h] (**9.73**)[f]	50	−0.82	–	–	–
	H_{II}[c]	5.25 (**6.06**)	80	−24.80	5.00 (**5.43**)	82	−24.94
14:0	L_{c1}	5.34, 2.67, 1.77, 1.32	20	−0.36	*na*	*na*	*na*
	L_{c2}	5.23	55	42.05	*na*	*na*	*na*
	L_β	5.65, 1.38	20	−3.41[h]	5.63	48	−3.01
	L_α	5.02, 2.49, 1.65, 1.23	55	−10.79	5.04	54	–[b]
	H_{II}[c]	5.68 (**6.56**), 3.24,2.80, 2.13, 1.87, 1.60, 1.54	65	−30.01	5.73 (**6.62**)	57	−36.78
15:0	L_{c1}	5.49,2.75,1.84	1	−0.32	*na*	*na*	*na*
	L_β	5.86, 1.49	11	1.86	5.69	57	−1.75
	L_α	5.81[h]	60	–[b]	–	–	–
	H_{II}[c]	5.85 (**6.76**), 3.38, 2.93	70	−34.06	5.47 (**6.32**)	63	−30.40
16:0	L_c	5.79,2.88,1.92	1	−0.04	*na*	*na*	*na*
	L_β[i]	6.14,3.06,2.04,1.54, 1.02	11	3.10	5.99	60	−2.99
		6.18	35	−2.60			
	H_{II}[c]	5.98 (**6.91**)	70	−37.53	5.44 (**6.28**)	68	−39.20
		5.74 (**6.63**), 3.31, 2.87	75				
17:0	L_β[i]	6.27	10	2.95	6.43	70	0.14
		6.34	30	−1.55			
	H_{II}[c]	5.71 (**6.60**)	80	−34.99	5.52 (**6.38**)	78	−35.40
18:0	L_β[i]	6.50	10	3.55	6.64	72	−2.26
		6.60	40	−2.20	–	–	–
	H_{II}	5.88 (**6.79**)	80	−37.30	5.72 (**6.61**)	73	−32.8
19:0	L_β[i]	6.7	10	3.27	6.83	75	−1.63
		6.8	40	−1.85	–	–	–
	H_{II}[c]	5.94 (**6.86**)	80	−41.45	5.66 (**6.54**)	78	−35.90

Table 2 (*Continued*)

CL	Phase	(A) d[a] (nm)	T (°C)	$s^T \times 10^{-3}$ (nm/K)	(B) d[a] (nm)	T (°C)	$s^T \times 10^{-3}$ (nm/K)
20:0	L_β[i]	6.94	10	2.43	7.09	77	−2.70
		7.0	40	−6.35			
	H_{II}[c]	5.76 (**6.65**)[h]	85	−35.79	5.63 (**6.50**)	78	−29.20

na - not applicable.

[a] The d=basis vector length for SAXS. SAXS measurements are ±0.05 nm.

[b] Insufficient data points.

[c] For the Q_{II} and H_{II} phases, the lattice parameter is shown in bold brackets. The two values for the Q_{II} phases represent points just above the L_α/Q^a_{II} and Q^a_{II}/Q^b_{II} phase transitions, respectively.

[d] $Im\bar{3}m$.

[e] $Ia\bar{3}d$.

[f] $Pn\bar{3}m$.

[g] Linear thermal expansion coefficients from the lattice parameters.

[h] Data obtained on cooling.

[i] The two values shown for the L_β phases for β-D-GalDAGs with chain lengths greater than 15 carbon atoms indicate the lower *d*-spacing obtained for the L_β phase, followed by that of the inflection point.

corresponding CSC-DSC measurements. Also, the XRD data presented here show no evidence of an additional phase between the L_α and Q^a_{II} phases, possibly because of the relatively large (5 and 10 °C) temperature increment between measurements that was used. Thus, the nature of this thermal event remains uncertain.

Continued heating of samples of *rac*-di-10:0- to 13:0-β-D-GalDAGs (Fig. 3) typically shows one or more additional peaks at 70–80 °C, which possibly correspond to Q^a_{II}/Q^b_{II} phase transitions (see below). At still higher temperatures in samples of *rac*-di-12:0 and di-13:0-β-D-GalDAGs, there is a further transition,

Table 3
WAXS spacings of 1,2-dialkyl-3-*O*-(β-D-galactopyranosyl)-*rac*-glycerols with 14, 15, 16 and 18 carbon chains

CL (C atoms)	Phase		WAX spacing (nm)	T (°C)	HC subcell $\angle\gamma$(°)	A (nm^2)[a]	V_T (nm^3)
14:0	L_{c1}	$\mathbf{T}_{\|\|}$[b]	**0.44, 0.38, 0.34,**	20	**106.8**	0.174	
		Other	0.58, 0.52				
	L_{c2}	$\mathbf{T}_{\|\|}$[b]	**0.44, 0.38, 0.34,**	58	**113.3**	0.184	
		$O_\perp$[b]	*0.42, 0.37*		*110.1*	*0.192*	
		L_β	0.415	20	120.0	0.199, 0.3958[c]	1.172
		L_α	0.45	55		0.4677[c]	1.174
		H_{II}	0.45	65			
15:0	L_{c1}	$\mathbf{T}_{\|\|}$[b]	**0.44, 0.38, 0.36,**	10	**110.4**	0.180	
		Other	0.49				
		L_β	0.414	20	120.0	0.198, 0.3958[c]	1.172
		H_{II}	0.46	70			
16:0	L_c	$\mathbf{T}_{\|\|}$[b]	**0.43, 0.38, 0.34**	0	**113.0**	0.188	
		$O_\perp$[b]	*0.403, 0.36*		*116.9*	*0.164*	
		L_β[b]	0.405		120.0	0.189, 0.3788[c]	1.201
		Other	0.72, 0.56				
		L_β[b]	***0.405***	15	120.0	0.189, 0.3788[c]	1.201
		H_{II}	0.45	75	–	–	–
18:0		L_β[b]	0.41	55	–	–	–
		H_{II}	0.45	80	–	–	–

WAX measurements are ±0.01 nm. For the WAXS peaks $\lambda/2\sin\theta$, where $\lambda = 0.154$ nm and 2θ = the total diffraction angle. Areas (A) are calculated for one chain (Eq. (1)).

[a] Corrected values using a tilt of 16° and $A = 2A_c/\cos\theta_{tilt}$ (Tristram-Nagle et al., 1993) are as follows: 14:0 $L_{\beta'}$, 0.207 nm^2; 15:0 $L_{\beta'}$, 0.206 nm^2; 16:0 $L_{\beta'}$, 0.197 nm^2. V_T is the hydrated volume.

[b] For the hydrocarbon chain subcell packing: $\mathbf{T}_{||}$ is the triclinic parallel subcell in regular bold, $O_\perp$ is the orthorhombic perpendicular subcell in regular italics. In the 16:0 mixed phase, the L_β phase is in bold italics.

[c] Areas (A) are calculated for two chains using $A_i = 2 \times 2(w_i)^2/\sqrt{3}$ and w_i is WAXS. Koberl et al. (1998) calculates 0.182 nm^2 for one chain in a hybrid triclinic or orthorhombic lattice (Hauser et al., 1981; Pascher et al., 1992) in the L_c phase, but also cites a molecular packing of 0.355 nm^2.

which SAXS measurements of the 1,2-*sn*- and 2,3-*sn*-di-12:0-β-D-GalDAGs (Zeb and Seddon, 2007, personal communication) show is a Q_{II}/H_{II} phase transition. In samples of the *rac*-di-12:0-β-D-GalDAG, the temperature of this phase transition is initially observed by DSC at ∼102 °C, but with continued heating and cooling cycles this decreases to ∼95 °C, probably reflecting the generally poor hydration characteristics of the lamellar phases of these *rac*-β-D-GalDAGs (see Section 4). With small increases in chain length, the temperature range over which the Q_{II} phase is evident and the temperature of H_{II} phase formation (T_h), gradually decrease. Thus, in the *rac*-di-14:0 and di-15:0-β-D-GalDAGs, the lamellar/nonlamellar phase transition observed at 60–65 °C is shown by SAXS to be an L_α/H_{II} phase transition.

Generally, the phase transitions seen on heating are reversible on cooling (Fig. 3). However, DSC cooling thermograms of the shorter chain compounds show fewer, weakly energetic, high temperature events, suggesting that the Q_{II} phases are supercooled and that there might be a difference in the number of Q_{II} phases seen on heating and cooling (see below). A comparison of the DSC measurements obtained from both calorimeters also shows that there is a significant difference in the temperature resolution of the Q_{II}/L_α phase transitions on cooling of the *rac*-di-12:0-β-D-GalDAG. Interestingly, although the SAXS measurements suggest the existence of an L_α phase on cooling in the di-13:0 lipid (Fig. 5), neither calorimeter was able to resolve a discrete Q_{II}/L_α phase transition.

Above a hydrocarbon chain length of 16 carbon atoms, the chain-melting and the L_α/H_{II} phase transitions are integrated into a single highly endothermic peak and thus T_m and T_h are the same. As was also evident in the shorter chain lipids, the values of T_m for the *rac*-di-16:0- to di-20:0-β-D-GalDAGs continue to increase with increasing chain length, reflecting the increasing stability of the L_β phase with increasing chain length (Fig. 4A; Table 1). The ΔH values of the chain-melting phase transitions (Fig. 4B) follow straight lines with similar slopes below a chain length of 15 carbon atoms and above a chain length of 16 carbon atoms, but there is a discontinuity between 15 and 16 carbon atoms, reflecting the combination of the L_β/L_α and L_α/H_{II} phase transitions at longer chain lengths. The difference in ΔH is −3.5 kcal/mol, which is greater than that of 1.5–2.0 kcal/mol seen in the di-15:0 lipid, suggesting the existence of an additional energetic contribution underneath the L_β/H_{II} phase transition.

On annealing of the *rac*-β-D-GalDAGs at either 4 or 22 °C for extended time periods (up to 2 years), samples with chain lengths from 10:0 to 18:0 carbon atoms all formed highly ordered L_c phases (see below). At shorter chain lengths ($N \leq 15$), the heating thermograms of annealed samples show two highly energetic endotherms (henceforth termed L_{c1} (lower temperature) and L_{c2} (higher temperature)), whose phase transition temperatures increase with increasing chain length, but which are consistently 10 °C apart (Figs. 3 and 4; Table 1). The ΔH values of both phase transitions from the L_c phase are highly energetic, exceeding the ΔH of the corresponding L_β/L_α phase transitions at chain lengths less than 15 carbon atoms. In the case of the di-10:0-β-D-GalDAG, the ΔH values of both the L_{c1}/L_{c2} and L_{c2}/liquid-crystalline phase transitions deviate from the expected line of regression, probably reflecting an increase in the headgroup H-bonding contributions at shorter chain lengths.

At higher temperatures, the L_{c2} phase converts to either an L_α phase ($N = 10$–13) or a H_{II} phase ($N = 14$,15). The heating thermograms of the CSC-DSC samples of the shorter chain lipids heated and cooled at 10 °C/h often showed an exotherm at a temperature below the two endothermic events. Using peak deconvolution methods devised 'in house' for Origin 7.5, we found that the area of the exotherm was approximately equal to that of the lower temperature endotherm corresponding to the L_{c1}/L_{c2} phase transition seen on heating. Despite repeated attempts using a variety of temperature protocols in our DSC experiments, we were unable to isolate the second endothermic component from the first. A comparison of the phase transition temperatures and ΔHs shows that while the L_{c2}/liquid-crystalline phase transitions occur at higher temperatures, they have lower ΔH values than the L_{c1}/L_{c2} phase transitions. However, while no odd–even alternation was evident in either the transition temperatures or the ΔH values of these phase transitions, there was significant odd–even alternation in the L_β/L_c conversion rate. This was faster in the even-chain lipids than in the odd-chain lipids, suggesting that differences in hydrocarbon chain end group packing probably determine the rate of the L_c phase formation, as has been observed in n-alkanes (Chevallier et al., 1999; Nakaoki et al., 2004; Li et al., 2004). At longer chain lengths ($N = 16$:0–18:0), the two endothermic events seen in the annealed shorter-chain lipids are replaced by a single endotherm at a temperature at, or below, the T_m (Fig. 3), probably arising from the transition from a single L_{c1} phase to a L_β phase. In *rac*-β-D-GalDAGs with a chain length greater than 18 carbon atoms, no corresponding lower temperature endothermic event was observed even after extended periods of annealing (up to 2 years) under suitable conditions, reflecting the slow L_β/L_{c1} phase conversion rate.

3.2. X-ray diffraction measurements

The X-ray diffraction patterns obtained for this series of *rac*-β-D-GalDAGs are generally consistent with the pattern of thermotropic phase behaviour observed by DSC and confirm the DSC transition temperatures. As a result of the complex pattern of solid-state polymorphism evident in the DSC thermograms and the rapid rate of L_β/L_c phase conversion, it was decided to collect data on the shorter chain compounds ($N \leq 14$) by performing the measurements in the cooling direction first and then to immediately reheat the samples as described above for the DSC measurements. This experimental protocol was successful in obtaining SAXS reflections for the metastable L_β phases of these shorter chain lipids (with the exception of *rac*-di-10:0-β-D-GalDAG) using the above generator/camera systems (Fig. 5). This protocol effectively reproduces a pattern of thermal events which closely resembles that seen at slower heating and cooling rates obtained using the CSC-DSC. Below, we present a structural overview of the L_c phases followed by a similar overview of the mesophases.

3.3. Lamellar-crystalline phases

On heating the shorter chain compounds, the supercooled L_β phase, which is characterized by low-angle reflections in the ratio 1:2:3:4 and by a single sharp wide-angle reflection[1] centred at 0.42 nm indicative of ordered, hexagonally packed hydrocarbon chains (Fig. 6A and inset), converts to the L_{c1} phase at temperatures corresponding to the exothermic events observed in the heating scans obtained using the CSC-DSC. In the small-angle region, this L_β/L_{c1} conversion is accompanied by a small decrease (0.2 nm) in the first-order spacing and by a change in the single wide-angle peak centered at 0.42 nm to two strong and sharp (0.44, 0.38 nm) and one very weak (0.34 nm) reflection (Fig. 6D and inset, Tables 2 and 3), suggesting a change in the hydrocarbon chain packing from a hexagonal to an untilted triclinic parallel ($T_{||}$) subcell (Chapman, 1965; Luzzati, 1968). Additional heating results in a further small decrease (0.15 nm) in the first-order spacings at the L_{c1}/L_{c2} phase transition and a change in the wide-angle diffraction pattern to one consisting of three strong, sharp reflections (0.44, 0.42 and 0.38 nm) and two weaker (0.37 and 0.34 nm) reflections. However, whereas the negative change in the L_{c1} phase linear thermal expansion coefficient (*s*, Table 2) is relatively small, it is not clear whether the corresponding change for the L_{c2} phase is also small. This is because of both insufficient data points prior to the chain melting phase transition and an apparent increase in the slope between the calorimetrically measured L_{c1}/L_{c2} and L_{c2}/L_α phase transition temperatures in the di-11:0-, di-13:0- and di-14:0-β-D-GalDAGs. This behaviour possibly originates from a small change in hydrocarbon chain tilt on going from the L_{c1} to the L_{c2} phase, as has been found for the corresponding 1,2-*sn*-β-D-GalDAG (Seddon et al., 2003; Koberl et al., 1998).

At longer chain lengths, where the temperatures of the L_{c1}/L_{c2} and L_{c2}/liquid-crystalline phase transitions coincide with those of the L_β/L_α phase transition, and because the rate of L_β/L_c phase conversion is also slower, it becomes more difficult to determine the phase identity and order. This is particularly true of samples of *rac*-di-15:0- and di-16:0-β-D-GalDAG. The DSC results suggest that both the L_{c1} and L_{c2} phases are present in the di-15:0 lipid, but, on the timescale of our experiments, SAXS/WAXS measurements have only found reflections consistent with an L_{c1} phase (Fig. 6E inset), supporting the observation of odd–even chain kinetic effects as seen by DSC.

We should emphasize that we have not performed WAXS measurements on the entire homologous series of *rac*-β-D-GalDAGs, but have chosen lipids with different chain lengths whose thermotropic phase behaviour is typical of the series and thus some of the phase assignments presented here should be considered as tentative.

A comparison of the L_{c1} SAXS patterns for the di-14:0 and di-15:0 lipids show some significant differences. Firstly, there are fewer reflections in the low-angle region for samples of the di-15:0 lipid (three reflections) than the di-14:0 lipid (four reflections), possibly caused by a difference in bilayer long-range order with increasing chain length (insets Fig. 6D and E). This is accompanied by differences in the position and intensity of the reflections in the wide-angle region. Specifically, while the first reflection seems equally intense in both lipids, the second and third reflections of the L_{c1} phase in the di-15:0 lipid are closer together and are also of similar intensity, whereas the second reflection is much stronger in intensity than the third reflection in the di-14:0 lipid (inset Fig. 6D). This suggests that differences in hydrocarbon chain end group contributions may be distorting the chain packing in the $T_{||}$ subcell of the odd-chained lipid (Tenchov et al., 1999).

[1] Although the *d*-spacing values in the text are rounded, some values shown in Table 2 are given to three decimal places. This permits differentiation between distinct diffraction peaks which are in close proximity. The error margins provided in the text are generous and the reporting of the additional decimal place in Table 2 does not reflect a corresponding increase in accuracy.

The corresponding WAXS diffraction patterns for the L_c phases of the di-16:0-β-D-GalDAG consist of a mixture of at least three diffraction profiles, one L_β reflection at 0.405 nm, an L_{c1} diffraction pattern (0.43, 0.38, 0.34 nm) and an L_{c2} diffraction pattern (0.403, 0.36 nm). This complicated mixture of phases in consistent with the DSC data shown in Fig. 3. Using thermogram peak deconvolution techniques, two endothermic components could be distinguished, in addition to that of the L_β/H_{II} phase transition, separated by only 5 °C (63–68 °C). The lower temperature component probably corresponds to an L_{c1}/L_{c2} phase transition, while the higher temperature component may originate from an L_{c2}/H_{II} phase transition. The difference in the WAXS diffraction patterns observed for the di-14:0- to di-16:0-β-D-GalDAGs (inset Fig. 6D–F; Table 3) shows an obvious decrease in the rate of L_c phase formation with increasing chain length. It is also interesting that the di-15:0-β-D-GalDAG only forms an L_{c1} phase on the time scale of the WAXS experiments, also supporting the observation that the kinetics of the L_{c1}/L_{c2} phase conversion process is slower in the odd-chained compounds.

The variations in peak intensity and peak position in the wide-angle region clearly reflect small differences in hydrocarbon chain packing of the above L_c phases. Details of the lateral hydrocarbon chain packing modes of these phases can be calculated using Eqs. (1) and (2):

$$s_{hk}^2 = ha^{*^2} + kb^{*^2} - 2hka^*b^* \cos\gamma, \quad (1)$$

where a^* and b^* are the magnitudes of the reciprocal lattice vectors and γ is the angle between them, and:

$$A = (a^*b^* \sin\gamma)^{-1}, \quad (2)$$

where A is the area of the unit cell in real space (nm^2). These calculations provide the dimensions of the hydrocarbon chain unit cell and the area per chain measured perpendicular to the chains. Corresponding values for the area per molecule calculated from the WAXS spacings, using an alternative procedure, are also given in Table 3 (see table footnotes for details).

For the L_{c1} phase in the *rac*-di-14:0-β-D-GalDAG, there are three peaks at 0.44, 0.38 and 0.34 nm (all ± 0.01 nm^2, see Fig. 6D inset upper profile), indicative of a $T_{||}$ packing mode. Letting $a^* = 1/(0.44\,\text{nm})$, $b^* = 1/(0.38\,\text{nm})$ and $s_{11} = 1/(0.34\,\text{nm})$, then $\gamma = 107°$ and $A = 0.174 \pm 0.01$ nm^2.

For the L_{c2} phase in the *rac*-di-14:0-β-D-GalDAG, the WAXS data suggest a hybrid subcell (Mannock et al., 1994; Chevallier et al., 1999; Nakaoki et al., 2004; Li et al., 2004; Chapman, 1965; Luzzati, 1968; Seddon et al., 2003) as described above. The $T_{||}$ unit cell is essentially the same as the L_{c1} phase above. The orthorhombic perpendicular ($O_\perp$) unit cell is represented by two peaks at 0.42 and 0.37 nm (all ± 0.01 nm), respectively. Letting $a^* = b^* = 1/(0.42\,\text{nm})$ and $s_{11} = (1/0.37\,\text{nm})$, we obtain $\gamma = 110°$ and $A = 0.192 \pm 0.01$ nm^2 (see the additional data summarized in Table 2).

Similarly, for the L_{c1} phase in the *rac*-di-15:0-β-D-GalDAG, there are three peaks at 0.44, 0.38 and 0.36 nm (all ± 0.01 nm, see Fig. 6E inset). Letting $a^* = 1/(0.44\,\text{nm})$, $b^* = 1/(0.38\,\text{nm})$ and $s_{11} = (1/0.36\,\text{nm})$, then $\gamma = 110°$ and $A = 0.180 \pm 0.01$ nm^2. The minimum area per hydrocarbon chain based on studies of chain packing in alkanes, triglycerides and fatty acids is thought to be 0.182 nm^2 (Abrahamsson et al., 1978). The values calculated here fall in the range 0.174–0.190 nm^2, in agreement with values obtained for the corresponding 1,2-*sn*-β-D-GalDAGs (Koberl et al., 1998) and PEs (Seddon et al., 1984; Pascher et al., 1992; Hauser et al., 1981).

Although we observed endothermic phase transitions below the T_m in our DSC experiments of the *rac*-di-17:0- and di-18:0-β-D-GalDAGs, we were unable to induce the formation of the L_c phases in either lipid on the time scale of our WAXS experiments. Thus, we only report *d*-spacings of the L_β and H_{II} phases of lipids with chain lengths greater than 17 carbon atoms. As might be expected, those increase in line with the values obtained for the shorter chain lipids (Fig. 7).

Plots of the *d*-spacings for the lamellar phases of the *rac*-β-D-GalDAGs just below their respective phase transitions, together with those of the corresponding 1,2-*sn*-β-D-Gal and β-D-GlcDAGs and the PEs, appear in Fig. 7A and B. The *d*-spacing values for the L_c phases for all of the lipids have almost identical slopes as a function of chain length and differ only slightly in their dimensions. The slope of the lines of regression through each lipid data set is ~0.25 nm/CH_2, which corresponds to a phase structure in which the chains are untilted (Chapman, 1965; Luzzati, 1968; Hauser et al., 1981).

3.4. Lamellar and nonlamellar liquid-crystalline phases

The plots of the long spacings of the *rac*-β-D-GalDAG homologous series as a function of temperature are shown in Fig. 5. For most *rac*-β-GalDAGs studied (except di-10:0, which forms an L_{c1} phase), the SAXS measurements at temperatures below the major endothermic event seen in unannealed lipid samples by DSC, show a series of low-angle reflections in the ratio 1:2:3:4, consistent with a lamellar phase, which is most probably a L_β phase (see below). At temperatures above

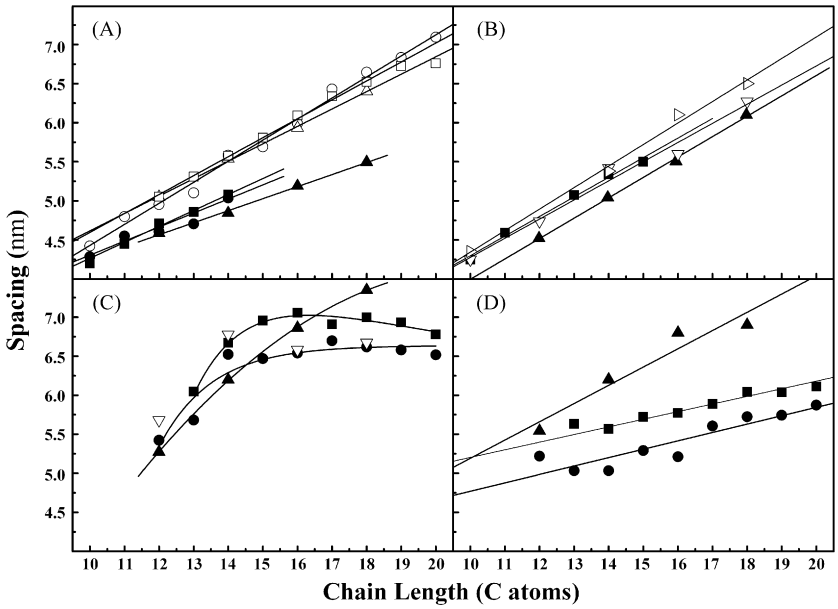

Fig. 7. A plot of the lattice basis vector (***a***) vs. chain length for a series of racemic dialkyl-β-D-galactosyl- and β-D-glucosyl-glycerols (Mannock et al., 2000) and the 1,2-*sn*-dialkyl-phosphatidylethanolamines (Seddon et al., 1984; Prof. John Seddon, unpublished data) measured on either side of the respective phase transitions. (A) The L_β and L_α spacings. (B) The L_c phase spacings. (C) The lattice parameter of the H_{II} phase measured at T_h. (D) The lattice parameter of the H_{II} phase extrapolated to 100 °C (as per ref. Koberl et al., 1998; Tenchova et al., 1996). *Symbols*: In panel A, the open symbols are the L_β phase, the closed symbols are the L_α phase and indicate the following lipids: *rac*-Gal (■), (□); *rac*-Glc (●), (○); PEs (▲), (△); uncorrected 1,2-*sn*-β-D-GalDAGs (▷) and uncorrected 1,2-*sn*-β-D-GlcDAGs (▽) (Hinz et al., 1991; Koberl et al., 1998; Tenchova et al., 1996; Mannock et al., 1994). The same symbols are used in panels B–D. The fits in panels A, B and D are linear, those in panel D are polynomial fits. For details of s^{CL} and s^0 see Table 4.

the L_β and/or L_c phases, several liquid-crystalline phases are formed whose geometry is both temperature and chain length dependent. On continued heating of the shorter chain compounds ($N \leq 13$) to temperatures above the L_{c2} phase, there are further small decreases in the characteristic lamellar low-angle reflections, consistent with the formation of a lamellar phase, which is probably a L_α phase (Fig. 6B; Table 2. Also see the WAXS data below). Although, Koberl et al. (1998) have reported that the thermal expansion coefficients of the L_β phases in these *rac*-β-GalDAGs are only weakly temperature dependent, we have found that, over a wider range of temperature, the L_β phase *d*-spacing initially increases, reaching a maximum at 35–40 °C, then decreases with increasing temperature up to the chain-melting phase transition. This observation appears to correspond to a decrease in the number of reflections in the wide-angle region (data not shown), possibly reflecting a decrease in L_β phase order with increasing temperature. In contrast, the linear thermal expansion coefficient of the L_α phases decreases significantly with increasing temperature, reflecting the gradual decrease in chain length with increasing temperature (Table 2), as was observed in the corresponding 1,2-*sn*-glycoglycerolipids (GGLs) (Koberl et al., 1998).

Further heating of these shorter chain *rac*-β-D-GalDAGs shows a significant increase in the low-angle spacings, as well as a change in the position of the associated long spacings. Immediately above the transition from the L_α phase, a mixed phase region consisting of two Q_{II} phases is formed, one of which has reflections in the ratio $\sqrt{2}{:}\sqrt{3}{:}\sqrt{4}{:}\sqrt{6}{:}\sqrt{8}{:}\sqrt{9}$ characteristic of a $Pn\bar{3}m$ phase (space group Q^{229}). At lower temperature, the lattice parameters in the cubic phase region decrease sharply with increasing temperature, whereas the corresponding cooling measurements show a straight, linear expansion of the $Pn\bar{3}m$ lattice over the entire cubic phase region. On cooling, the lattice parameters are consistent with those seen in the high temperature region on heating. Also, calculation of the Q^a_{II} and Q^b_{II} lattice parameters at the Q^a_{II}/Q^b_{II} phase transition temperatures (Table 2) as a function of chain length show that the Q^a_{II} phase dimensions decrease more rapidly with increasing chain length ($s^{CL} = -0.245$ nm/CH_2, $s^0 = 11.46$ nm (where s^{CL} is the chain length dependent expansion coefficient of the relevant phase and s^0 is the extrapolation

of the phase dimensions to zero chain length) than do those of the Q_{II}^{b} phase dimensions over the same range of chain lengths ($s^{CL} = -0.094$ nm/CH_2, $s^0 = 9.38$ nm).

Typically, in NL phases, there are both hydration and chain length-dependent curvature contributions to the lattice parameter (see below) and these various contributions cannot be readily deconvolved without more extensive SAXS experiments. Nevertheless, the above observations support the idea that two Q_{II} phases are seen on heating, but only a single Q_{II} phase is seen on cooling, as was found in our earlier glycolipid studies (Mannock et al., 2001a, 1992, 2000). There are insufficient diffracted orders to definitively identify the first Q_{II} phase seen on heating. It may be either an $Ia\bar{3}d$ phase (space group Q^{230}, $a = \sqrt{2}d$), as was observed in the our earlier studies of the *rac*-1,2-di-12:0-β-D-GlcDAG (Turner et al., 1992; Lewis et al., 1997), or, more likely, an $Im\bar{3}m$ (space group Q^{224}, $a = \sqrt{6}d$), as has been observed in studies of PEs, 1,2-*sn*-dialkyl- and diacyl-β-D-GalDAGs (Mannock and McElhaney, 1991; Koberl et al., 1998; Seddon et al., 1984; Zeb and Seddon, personal communication). Others have recently reported rhombohedral and $P4_332$ cubic phase intermediates in phosphatidylcholine/water and monoglyceride/water mixtures (Yang and Huang, 2003; Kraineva et al., 2005), which may explain the additional reflections seen just above the L_α phase in our studies of the *rac*-β-D-GlcDAGs (Mannock et al., 2000).

In the present study, it was found that the number and position of DSC peaks in the Q_{II} phase region varied with the number of heating and cooling cycles and that the initially observed behaviour could be restored by cooling and annealing of the sample allowing formation of the L_c phase. Thus, these discrepancies may be explained by variations in either the sample preparation employed by each group or the sample thermal history (Erbes et al., 1994), which may also be technique dependent. This is particularly true of lipids whose mesophases are not readily hydrated and which require repeated cycling to prepare homogeneously hydrated preparations and where the energetic barrier between Q_{II} phases is relatively small (Turner et al., 1992).

Additional heating of samples of the di-13:0-β-D-GalDAG shows a further change in the low-angle spacings to the order $1{:}\sqrt{3}{:}\sqrt{4}{:}\sqrt{7}{:}\sqrt{9}$ (Rivas and Luzzati, 1969; Shipley et al., 1973), characteristic of a H_{II} phase. Although the PE-DSC measurements were able to resolve a poorly energetic endotherm at a temperature between 92 and 102 °C in the *rac*-di-12:0-β-D-GalDAG (depending on the sample thermal history), our apparatus was not set up to perform the corresponding SAX measurement at this high temperature.

Support for the phase assignments in unannealed samples of the di-14:0–16:0-*rac*-β-GalDAGs is provided by a combination of SAXS and WAXS measurements. Below the major endothermic event seen by DSC in the di-14:0–16:0-*rac*-β-GalDAGs, the SAXS data is indicative of a lamellar phase. In the wide-angle region, there is a single sharp peak at 0.42 nm (±0.01 nm), indicative of a L_β phase with ordered hydrocarbon chains packed on a hexagonal lattice (Fig. 6A). For the di-14:0-*rac*-β-GalDAG, $a^* = b^* = 1/(0.415\text{ nm})$, $\gamma = 120°$, and therefore $A = 0.199 \pm 0.01$ nm^2 (Fig. 2; Table 3). At temperatures just above the L_β phase in di-14:0-*rac*-β-GalDAG, the SAXS data is still indicative of a lamellar phase, but the diffuse band at 0.45 nm in the wide-angle region of the same lipid is indicative of a L_α phase with disordered hydrocarbon chains packed in a hexagonal subcell (Fig. 6B). In the di-14:0–16:0-β-D-GalDAGs, at temperatures above the chain-melting phase transition, the Q_{II} phases seen at shorter chain lengths are absent. Instead, at both higher temperatures and longer chain lengths, the SAXS and WAXS diffraction spacings support the existence of an H_{II} phase (Fig. 6C). At longer chain lengths, the complex pattern of weakly energetic endothermic peaks arising from liquid-crystalline lamellar/nonlamellar phase transitions is replaced by a single highly energetic thermal event, which can be confidently assigned to a direct L_β/H_{II} phase transition. The lattice parameters, a, for the H_{II} phase of each lipid chain length are listed in Table 2 and are in good agreement with the values obtained for the corresponding dialkyl-β-D-GlcDAGs reported elsewhere (Mannock et al., 1992; Koberl et al., 1998; Turner et al., 1992).

4. Discussion

4.1. The effect of headgroup, interface and hydrocarbon chain length of the phase behaviour of dialkyl glycoglycerolipids

From Figs. 3 to 5, it is clear that the equilibrium phase behaviour of the *rac*-β-D-GalDAGs is dominated by the presence of two poorly hydrated L_c phases, one of which, the L_{c2} phase, contains hydrocarbon chains which are slightly tilted relative to the bilayer surface (Table 2), as has been reported for the 1,2-*sn*-β-D-GalDAGs (Seddon et al., 2003) and dialkyl PEs (Seddon et al., 1984). In contrast, the L_{c1} phase seems to be untilted, as was observed for the corresponding 1,2-*sn*-β-D-GlcDAGs (Seddon et al., 2003; Koberl et al., 1998) (see below). Fig. 4 shows the plots of the chain length dependence of the transition temperatures and associated enthalpy changes of the phase transitions from each

phase in these glycolipids. The phase transitions from the L_{c2} phase at shorter chain lengths ($N \leq 13$) are L_{c2}/L_α phase transitions, but at longer chain lengths the L_α phase is replaced by a H_{II} phase. There are no distinct odd/even discontinuities in the chain length dependence of the observed L_c/liquid-crystalline phase transition temperatures and associated enthalpy values. Odd–even alternation, which was a feature of the L_c phase transition temperatures of both the 1,2-*sn*-diacyl-α- and β-D-GlcDAGs (Mannock et al., 2001b, and references therein), is believed to originate from the formation of a strongly hydrocarbon chain-tilted, lamellar-crystal-like phase (Broadhurst, 1962). However, the diffraction profiles and SAXS and WAXS reflections of both the L_{c1} and L_{c2} phases in the *rac*-β-D-GalDAGs suggest that the structure of each phase is largely unaltered by increases in chain length, although a comparison of odd and even chain compounds suggests that there may be some distortion of the hydrocarbon chain packing which may contribute to the odd–even alternation in the kinetics of L_{c1} phase formation (Fig. 6D–F).

In unannealed *rac*-β-D-GalDAG samples, the metastable L_β and L_α phases exist at lower temperatures. The L_β/L_α transition temperatures and associated enthalpy changes are strongly chain length-dependent. When plotted as a function of hydrocarbon chain length (Fig. 4), both parameters show relatively smooth monotonic increases with hydrocarbon chain length without any discontinuities between the odd- and even-numbered homologues. This is generally what is expected of simple chain-melting phenomena, in which the melted phase (in this case the L_α phase) is nucleated from a loose, hexagonally packed structure (Broadhurst, 1962). However, a close inspection of Fig. 4B shows that the enthalpy values for the di-15:0- to di-20:0 compounds are slightly higher than an extrapolation of the enthalpy values at shorter chain lengths. This small additional contribution (with an expected range of 1.5–2 kcal/mol) can be attributed to the conversion of the L_β phase directly to the H_{II} phase. Unlike the dialkyl-*rac*-β-D-GlcDAGs, plots of the *rac*-β-D-GalDAGs L_β first-order spacings as a function of chain length indicate a slight tilt, but they are less tilted than the $L_{\beta'}$ phase of the corresponding dialkyl PEs (Seddon et al., 1984).

In the respective homologous series, the L_β/L_α phase transition temperatures are slightly higher in the *rac*-β-D-GalDAGs than in the *rac*-β-D-GlcDAGs for the same chain length, suggesting a more ordered L_β phase in the former, which is probably the result of poor headgroup hydration. Above the L_β/L_α phase transition, there is a gradual change in the temperature intervals between lamellar and nonlamellar phases with increasing hydrocarbon chain length seen on heating. The L_α phase disappears at a chain length of 16 carbon atoms in the *rac*-β-D-GalDAGs, but at a chain length of 15 carbon atoms in the *rac*-β-D-GlcDAGs. Given the poor hydration characteristics of the *rac*-β-D-GalDAGs, it is tempting to suggest that these differences arise from a headgroup directed, but chain length dependent re-entrant behaviour seen in the phase diagram of the didodecyl-*rac*-β-D-GalDAG (Turner et al., 1992), where at moderate hydration levels the L_α/Q_{II} phase transition temperature increased relative to both higher and lower water contents. This was attributed to a change in membrane curvature and subsequently to a change in headgroup hydration at lower water contents (Mannock et al., 1992; Turner et al., 1992; Di Gregorio and Mariani, 2005; and references therein).

In the shorter chain compounds, the chain length dependence of the lamellar liquid-crystalline to nonlamellar phase transitions is complicated because the number and nature of the nonlamellar phases formed are chain length dependent. Up to three nonlamellar phases were observed in the heating and cooling experiments of these β-D-GalDAGs, which we have been tentatively identified (in order of increasing temperature) as $Im\bar{3}m$, $Pn\bar{3}m$ and H_{II} phases, respectively, on the basis of their SAXS reflections. From Figs. 3 and 5, it is evident that the L_α/H_{II} phase transition temperatures seen at short chain lengths occur consistently at 60–70 °C; this is significantly higher than the corresponding measurements of *rac*-β-D-GlcDAGs, where no L_c phase polymorphism is evident (Mannock et al., 2000), suggesting that the β-D-Gal headgroup is not fully hydrated in these lipids even in the liquid-crystalline phases.

In these unannealed shorter chain *rac*-β-D-GalDAGs, the heating and cooling temperature window over which the cubic phases are stable is slightly greater than in the corresponding *rac*-β-D-GlcDAGs (Fig. 5), suggesting that the hydrated β-D-Gal headgroup is larger and that the Q_{II} phases have a lower curvature at the same chain length than those of the β-D-Glc headgroup in these circumstances (see below). However, it is the temperature of the transition to the H_{II} phase which decreases most markedly with increasing hydrocarbon chain length in both dialkyl GGLs. Effectively, the temperature window over which the lamellar and inverted cubic phases are stable decreases, whereas the stability of the H_{II} phase increases with increasing chain length, as was observed in our earlier measurements of the diacyl GGLs and those of other nonlamellar-preferring lipids (Lewis et al., 1997; Mannock and McElhaney, 2004, and references therein).

4.2. An analysis of the temperature and chain length dependence of the lamellar and nonlamellar phase dimensions at the respective phase transition temperatures

Estimation of the contributions of the various lipid bilayer components has typically been achieved by means of swelling experiments performed as a function of water concentration on a single lipid species. With the glycolipids, these experiments are very difficult to perform on all but the shortest chain lengths because, at equilibrium, the lipids tend to form L_c phases which do not swell significantly with increasing water content (Sen et al., 1990). In order to provide a more consistent analysis of the effect of headgroup structure on the lamellar and nonlamellar phase dimensions of both the dialkyl GGLs and PEs, we have calculated the lattice parameters of each phase at the appropriate phase transition temperatures as a function of chain length (Fig. 7). This approach is made possible because of the wide range of lipid headgroup structures and hydrocarbon chain lengths available in our laboratory. From these calculations, it is possible, by extrapolation to a lattice parameter at zero chain length, to produce an estimate of the headgroup/water contribution to the phase dimensions of a wide range of lamellar phases independent of hydrocarbon chain length.

A comparison of Fig. 7A and B clearly shows that the *d*-spacings of the L_β phases are typically 0.5–0.7 nm larger at the L_β/L_α phase transition temperature than those of the corresponding L_c phases. This arises mostly from a difference in the thickness of the water layer, d_w (Fig. 2), although in some lipids there is also a difference in hydrocarbon chain tilt between these two phases. A comparison of the L_β phase chain length-dependent expansion coefficients for the *rac*-β-Glc- and *rac*-β-GalDAGs, as well as the dialkyl PEs (Fig. 7A; Table 4), shows that the L_β phases of the *rac*-β-GlcDAGs are untilted. This is in agreement with the previously published results (Mannock et al., 1994; Seddon et al., 2003), whereas the $L_{\beta'}$ phases of the β-D-GalDAG[2] are slightly tilted. In comparison, the $L_{\beta'}$ phases of the PEs are highly tilted, having an angle of tilt of ∼28° (Chapman, 1965; Seddon et al., 1984). Similar calculations for the analogous L_{c1} phases show that they are untilted in the *rac*- and 1,2-*sn*-β-D-GlcDAGs (Mannock et al., 1994; Koberl et al., 1998) as well as in the 1,2-*sn*-β-D-GalDAGs, whereas the equilibrium L_{c2} phases in both the *rac*- and 1,2-*sn*-β-D-GalDAGs (Seddon et al., 2003) as well as in the dialkyl PEs (Seddon et al., 1984), are tilted. Corresponding calculations for the L_α phases show that those of the *rac*-β-D-GalDAGs are more ordered and probably less hydrated than those of the corresponding β-D-GlcDAGs and PEs (Table 4), in agreement with the observations above. The SAXS and DSC measurements of the GGLs studied here suggest that whether or not L_c phases are formed, and their rate of formation is determined by the hydrophobic/hydrophilic balance of the headgroups, and subsequently the strength and number of hydrogen bonds around the sugar ring and their ability to retain water at the headgroup/water interface.

This assumption is supported by recent computer models of hydrated glycosides, which show that the angle and strength of the H-bonds in glycosides depends on the balance of axial and equatorial OH groups around the ring, and more specifically on the orientation of the hydroxyls at OH-2 and OH-4 (Galema and Hoiland, 1991; Cheetham and Lam, 1996; Dashnau et al., 2005; Koynova et al., 1997; Kirschner and Woods, 2001; Fabri et al., 2005; Mason et al., 2005; Almond, 2005). Thus, weaker headgroup-water H-bonds will alter the ordering of water around the headgroup and its ability to retain water in its hydration sphere. Recent molecular dynamics simulations of the corresponding alkyl glycoside surfactants (Chong et al., 2006) found that while there are many similarities in the measured and calculated hydration properties of the octyl-β-D-galactoside and octyl-β-D-glucoside, the β-D-Gal headgroup has a shorter water residence time and a greater tendency to form intramolecular H-bonds, suggesting that the β-D-Gal and β-D-Glc headgroups differ in the balance between solute–solute and solute–solvent interactions and thus their hydrophobic/hydrophilic balance. Experimental support of this idea is provided by density and ultrasound measurements of the corresponding methyl-D-glycosides (Galema and Hoiland, 1991; Kirschner and Woods, 2001). In addition, the homology of L_c phases in GGLs with different headgroups and interfacial chiralities and differences in their rates of L_c phase formation strongly indicates that the relative position of the glycerol 0–2′ is the key substituent which perturbs the headgroup hydrogen bonding network promoting L_c phase formation (Figs. 3 and 5) (Mannock et al., 1992, 1994, 2000; Seddon et al., 2003).

While the motionally averaged L_β and L_α phases may have similar dimensions at shorter chain lengths in GGLs with different headgroups (Fig. 7A), those dimensions may change with increasing chain length owing to differences in the headgroup hydrophobic/hydrophilic balance

[2] These values are only approximate because additional X-ray scatter at shorter chain lengths, due to the rapid formation of L_c phases in the *rac*-β-GalDAGs, added error to the measurements.

Table 4
The effect of headgroup structure on the increase in lattice parameter per methylene group (s^{CL}, nm/CH_2), angles of molecular tilt (∠°), the phase lattice parameters at zero chain length (s^0, nm) and bilayer hydrocarbon chain distance (D_c, nm) in both lamellar and nonlamellar phases measured at the phase transition

Head group	Phase																
	L_{c1}				L_β				L_α			Q_{II}^a		Q_{II}^b		H_{II}[a]	
	s^{CL}	∠	s^0	D_c (CL)	s^{CL}	∠	s^0	D_c (CL)	s^{CL}	s^0	D_c (CL)	s^{CL}	s^0	s^{CL}	s^0	s^{CL}	s^0
β-D-Gal	0.252	0	1.79	2.51 (10)	0.242	16	2.17	– (10)	0.204	2.22	1.98 (10)	−0.245	11.46	−0.094	9.38	0.098	4.23
				2.80 (11)				2.65[b] (11)			2.23 (11)						
				– (12)				2.89 (12)			2.49 (12)						
				3.28 (13)				3.14 (13)			2.64 (13)						
				3.55 (14)				3.40 (14)			2.86 (14)						
				3.71 (15)				3.64 (15)			– (15)						
				4.00 (16)				3.92 (16)			– (16)						
				– (17)				4.17 (17)			– (17)						
				– (18)				4.35 (18)			– (18)						
				– (19)				4.56 (19)			– (19)						
				– (20)				4.59[c] (20)			– (20)						
β-D-Glc	0.253[d]	0	1.70[d]	2.51 (10)	0.256	0	1.95	2.47 (10)	0.180	2.50	1.78 (10)	−0.217	19.39	0.075	7.16	0.107	3.70
				– (11)				2.85 (11)			2.05 (11)						
				3.00 (12)				3.00 (12)			2.11 (12)						
				– (13)				3.15 (13)			2.20 (13)						
				3.68 (14)				3.63 (14)			2.54 (14)						
				– (15)				3.74 (15)			– (15)						
				3.86 (16)				4.04 (16)			– (16)						
				– (17)				4.47 (17)			– (17)						
				4.53 (18)				4.69 (18)			– (18)						
				– (19)				4.88 (19)			– (19)						
				– (20)				5.14 (20)			– (20)						
PE	0.253	0	1.49	3.06 (12)	0.223	28	2.39	2.68 (12)	0.148	2.80	1.79 (12)	ND	ND	ND	ND	0.234	2.86
				3.55 (14)				3.15 (14)			2.05 (14)						
				4.03 (16)				3.56 (16)			2.39 (16)						
				4.61 (18)				4.01 (18)			2.7 (18)						

[a] Measured at 100 °C.
[b] One available data point.
[c] This low value may be an indication of incomplete hydration.
[d] 1,2-*sn* (Koberl et al., 1998). PEs (Seddon et al., 1984).

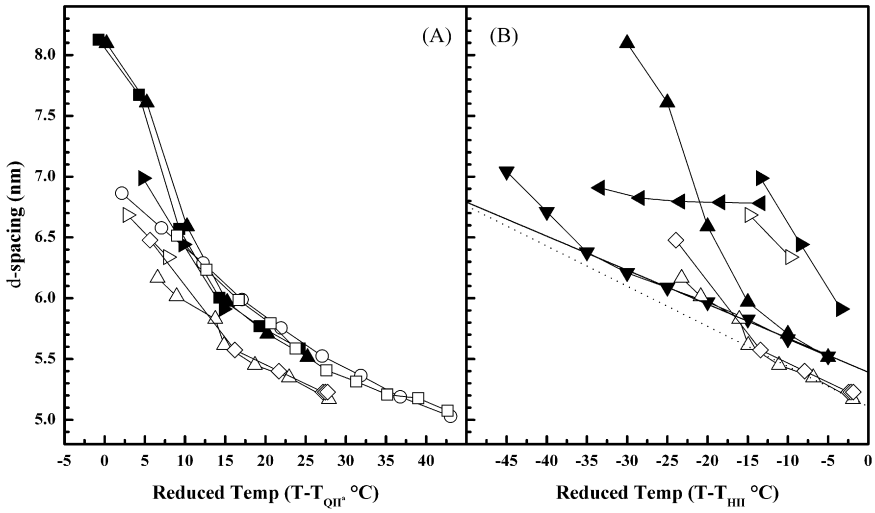

Fig. 8. A plot of the cubic phase *d*-spacings (nm) as a function of reduced temperature: (A) at T-T_{QII} and (B) at T-T_h. The symbols are as follows: filled symbols are β-D-Gal, empty symbols β-D-Glc, at the following chain lengths 10:0 (○); 11:0 (■, □); 12:0 (▲, △); 12:0 (Turner et al., 1992; ◊); 13:0 (►, ▷). The two linear lines of regression (β-D-Gal solid, β-D-Glc dashed) indicate the change in the $Pn\bar{3}m$ phase dimensions as a function of temperature. The corresponding thermal expansion coefficients appear in Table 2.

and its effect on d_w (Fig. 2). Again this is supported both by the density and ultrasound measurements of methyl-glycosides and the molecular dynamics simulations of the octyl-glycosides (Chong et al., 2006).

A comparison of the Q_{II} phase *d*-spacings in Fig. 8 shows that both Q_{II} phases appear to be larger in the β-D-GalDAGs just above the transition from the L_α phase, decreasing by as much as 3.5 nm over a range of 30 °C. The corresponding measurements of the β-D-GlcDAGs show a similar decrease in dimensions as a function of temperature, but are generally spread over a wider range of temperature than the corresponding β-D-GalDAGs. In fact, this narrower range of Q_{II} phase stability in the β-D-GalDAGs probably results from the existence of L_c phases at lower temperatures and the difficulty of achieving full hydration with increasing temperature which, because of the L_β/L_c phase conversion kinetics, may be chain length dependent. This is supported by the observation that the range of Q_{II} phase temperature stability is lower for the 10:0 and 11:0 β-D-GalDAGs, whereas the range of the Q_{II} phases for the di-12:0- and di-13:0-β-D-GalDAGs is approximately equal to that observed in the corresponding β-D-GlcDAGs.

At the low temperature end of the cubic phase region in both GGLs, there are significant differences in the Q^a_{II} *d*-spacings that are chain length dependent; those of the β-D-GalDAGs are significantly larger than those of the corresponding β-D-GlcDAGs. The lattice parameter linear thermal expansion coefficients, s^T, are also different in the two GGLs. Those of the β-D-GalDAGs are significantly greater than those of the corresponding β-D-GlcDAGs (Fig. 5; Table 2, lattice parameters, and Fig. 8, *d*-spacings) (Mannock et al., 2000), but appear to be internally consistent and do not change greatly with increasing chain length. On a reduced temperature scale (T-$T_{Q^a_{II}}$, Fig. 8A), the superimposition of the Q^a_{II} phase *d*-spacings of each β-D-GalDAG chain length ($n = 11$–13) and for those of the corresponding β-D-GlcDAGs ($N = 10$–13) shows the temperature dependent change in dimensions as more visible, as is the convergence of the Q^a_{II} and Q^b_{II} phase *d*-spacings at a reduced temperature of 15–20 °C in both GGLs. Whether or not these disparities are an indication of different Q^a_{II} phase geometry (β-D-GalDAGs, $Im\bar{3}m$ (Koberl et al., 1998; Mannock et al., 2001b) versus β-D-GlcDAGs, $Ia\bar{3}d$; (Turner et al., 1992) or water composition (Rappolt et al., 2006) just above the L_α/Q_{II} phase transition temperature is uncertain. The larger s^T values in the β-D-GalDAGs suggest that the two headgroup configurations may initially differ in their ability to counterbalance the splay of the hydrocarbon chains and thus the interfacial curvature with increasing temperature and that, in the β-D-GalDAGs, the increased order of the L_α phase and the poor headgroup hydration properties, and consequently the lipid hydrophobic/hydrophilic balance, modifies the phase curvature and dimensions, as has recently been proposed for the $Im\bar{3}m$ phase of some block co-polymers (Fang et al., 2006).

At higher temperature, on the reduced temperature scale (T-$T_{Q^a_{II}}$; Fig. 8A), the *d*-spacings of the $Pn\bar{3}m$ phase are on average slightly larger in the β-D-GalDAGs than in the β-D-GlcDAGs, whereas the corresponding s^T val-

ues are virtually identical. This supports the idea that the higher temperature cubic phase in these two GGLs is the same. The linear thermal expansion coefficients are similar in both the β-D-Gal- and β-D-Glc- containing lipids irrespective of chain length. By changing the reduced temperature scale from $T\text{-}T_{Q_{II}^a}$ to $T\text{-}T_{H_{II}}$ (Fig. 8B), the difference in the Q_{II}^b *d*-spacings with increasing chain length in the β-D-GalDAGs and the similarities in their s^T values at the transition to the H_{II} phase become more apparent. At the same chain length, the $Pn\bar{3}m$ phase *d*-spacings in the β-D-GalDAGs are also larger than those of the β-D-GlcDAGs. Thus, again there appears to be both a headgroup and hydrocarbon chain contribution to the phase dimensions and the linear thermal expansion coefficients (see below) and those structural components also determine the L_α/Q_{II} phase transition temperature and the temperature range over which the Q_{II} phases are stable.

The lattice parameters for the H_{II} phases observed in several of the β-D-GalDAGs are also chain length dependent and typically show a decrease of approximately 0.5 nm on heating over a temperature interval of 20 °C (Fig. 5; Table 2). The values in the 13–20 carbon chain length β-D-GalDAGs are larger than those of the β-D-GlcDAGs (Figs. 5 and 7C; Table 2). A similar variation in the repeat distance of the H_{II} phase as a function with temperature and water content has been reported for a polyunsaturated β-D-galactosyl diacylglycerol (Shipley et al., 1973) and for the *rac*-di-dodecyl-β-D-GlcDAG (Turner et al., 1992). The lattice parameters of the H_{II} phases measured at T_h (Fig. 7C) reach a maximum at a chain length of 16 carbon atoms. At longer chain lengths, they appear to gradually decrease, in agreement with the observations of the corresponding 1,2-*sn* diastereomers (Koberl et al., 1998), suggesting that the hydration of the lamellar and H_{II} phases may also be compromised at these long chain lengths. However, when the lattice parameter for each chain length is extrapolated to 100 °C (Fig. 7D), the spacings fall on straight lines of similar slope for the Gal and Glc lipids, but once again the H_{II} phase dimensions are larger for the β-D-GalDAGs than the β-D-GlcDAGs.

This suggests that the β-D-GalDAGs headgroup is better able to counterbalance the effects of increasing hydrocarbon chain splay with increasing temperature. A comparable plot of the corresponding PEs (Seddon et al., 1984) has a totally different slope. This suggests that if these measurements reflect a headgroup and hydration component at higher temperatures, the β-D-glucose headgroup is more "compact" with a less compressible hydration sphere in which the water is more strongly hydrogen bonded to the headgroup. This would favour a greater interfacial curvature than either the β-D-galactose or PE headgroups such that the hydration component of the two glycolipids behaves in a similar manner, possibly reflecting the similar hydration numbers of the corresponding methyl-glycosides (Galema and Hoiland, 1991; Cheetham and Lam, 1996; Dashnau et al., 2005; Chong et al., 2006) (see our discussion above), and thus their similar chain length dependent behaviour.

These observations are supported by studies (Koynova et al., 1997) which showed that a greater concentration of the kosmotropic solute, NaSCN, which disrupts the existing H-bonded water-solute structure, is required to induce a $L_\beta \rightarrow L_\alpha/Q_{II} \rightarrow H_{II}$ phase sequence in the di-16:0-β-D-ManDAG than for the corresponding β-D-GlcDAG lipid, suggesting that lipids containing these nonionic monosaccharides differ in the stability of their headgroup and interfacial hydration spheres. Fig. 8C and D also suggests that the headgroup and hydration contribution to the H_{II} phase *d*-spacings with increasing chain length is totally different for the GGLs and PEs (Seddon et al., 2003; Koberl et al., 1998).

It has been suggested that the differences in phase properties for glycolipids and PEs originate from a fundamental difference in the temperature dependent hydration properties of the respective lipid headgroups. Specifically, the glycolipid polar headgroup and interfacial hydration contribution decreases with increasing chain length (and thus the hydrophilic/hydrophobic balance), whereas that of the PE headgroup decreases to a much lesser degree. This may reflect the greater flexibility of the chain-like headgroup, the lateral repulsion of the neighbouring charged PO^{2-} and NH^{3+} groups, and their combined hydration properties (Koberl et al., 1998). Thus, the hydrophobic/hydrophilic balance of the PE headgroup is governed largely by attractive and repulsive coulombic interactions between headgroups, rather than van der Waals forces and hydrogen bonding interactions, which are the major contributors in the GGLs.

Interestingly, the influence of the latter contributions is evident on comparing the H_{II} lattice parameters of the 1,2-*sn*-β-D-GalDAGs, which are smaller than those of the corresponding 1,2-*sn*-β-D-G1cDAGs. Unlike in the *rac*-β-D-GalDAGs studied here, those results are probably a reflection of the lower level of hydration of the β-D-Gal headgroup relative to the β-D-Glc headgroup in the 1,2-*sn*-β-D-GalDAGs. This is brought about by the greater capacity of the *sn*-2 oxygen group to destabilize the β-D-Gal headgroup H-bonding interactions in favour of an intramolecular H-bond than the corresponding β-D-Glc headgroup, a mechanism which prevails in the formation of the L_c phases. This dehydration contribution has also been observed in the reentrant Q_{II} and

H_{II} phase behaviour in the *rac*-di-dodecyl-β-D-GlcDAG (Turner et al., 1992) and in di-oleoyl-PE (Di Gregorio and Mariani, 2005; and references therein). This mechanism may explain why the H_{II} phase lattice parameter of the 1,2-di-tetradecyl-3-*O*-(β-D-Gal)-*sn*-glycerol just above the L_α/H_{II} phase transition is smaller on heating than on cooling and is also smaller on heating than was observed at the same phase transition temperature in either the 2,3-di-tetradecyl-3-*O*-(β-D-Gal)-*sn*-glycerol or the diastereomeric mixture (Mannock et al., 1994).

These explanations of the effect of the sugar headgroup configuration on both the L_c and nonlamellar phase behaviour are consistent with studies of the phase behaviour of the 1,2-di-tetradecyl-3-*O*-(3-*O*-methyl-β-D-Glc-glycerol (Trouard et al., 1994) and the corresponding β-D-xylopyranoside (Seddon et al., 1996). In the former, where there is a larger but more hydrophobic headgroup, a poorly hydrated L_c phase is formed at lower temperature, whereas a highly curved, micellar Q_{II} (L2) phase is formed at higher temperature. In the corresponding β-D-xylopyranoside, the headgroup is smaller, but more hydrophilic. No L_c phases are formed at lower temperatures, whereas an $Fd\bar{3}m$ phase is formed at higher temperatures. Thus, at lower temperatures in the GGLs, an increase in headgroup size may be counteracted by an increase in hydrophobicity.

At higher temperatures in the motionally averaged lamellar phases, the hydrated headgroups have different patterns of strongly and weakly H-bonded water molecules and the headgroup–headgroup spacing is determined by the motion of the hydrocarbon chains. In the nonlamellar phases, the phase geometry is determined by the headgroup compressibility, which is controlled by "headgroup size" and the packing of its hydration sphere and the ability of those components to counterbalance the splaying of the hydrocarbon chains. These observations explain why the phase morphology and thermodynamic properties of the glycolipid mesophases may be similar in the β-D-GalDAGs and β-D-GlcDAGs, why those phases differ in their range of temperature stability, and why they differ in their ability to lose water when forming L_c phases at lower temperatures. It also explains the differences in the lamellar and nonlamellar phase polymorphism in the GGL diastereomers (Mannock et al., 1992, 1994; Kuttenreich et al., 1993); in the 1,2-*sn* diastereomer the glycerol O-2′ atom perturbs the headgroup and interfacial hydration and the headgroup conformation is restricted in the 2,3-*sn* diastereomer. Our measurements strongly support this interpretation, yet are consistent with previous observations of glycolipid phase behaviour (Koberl et al., 1998; Lewis et al., 1997, and references therein) and support the proposal (Mannock et al., 2001a; Harper et al., 2001) that it is the hydrocarbon chains that determine the area per molecule in the lamellar gel and lamellar liquid-crystalline phases, but it is the headgroup which determines the area per molecule in the NL phases.

5. Conclusions

For the first time, comparative measurements have been made on two homologous series of *rac*-dialkyl-MGDGs containing two different headgroups, β-D-galactose and β-D-glucose, and either two odd or two even alkyl chains. Using such a wide range of chain lengths, it has been possible to assemble a more extensive overview of the patterns of lamellar and nonlamellar phase polymorphism than has previously been reported.

The polymorphism of these *rac*-β-D-GalDAG's is dominated in both the crystalline and liquid-crystalline phases by a balance between headgroup and hydrocarbon chain packing effects, similar to those seen in the 1,2-*sn*-β-D-GalDAG's (Koberl et al., 1998; Tenchova et al., 1996). The rate of L_c phase formation, with its accompanying dehydration and in some cases hydrocarbon chain tilt, is dependent on the headgroup structure. Lipids containing a β-D-Gal headgroup lose water and adopt a hydrocarbon chain tilted conformation in the L_c phase more readily than those containing a β-D-Glc headgroup. Supporting measurements and simulations from related systems suggest that the water molecules in the hydration shell are more tightly bound to the β-D-Glc headgroup than in the β-D-Gal headgroup which readily forms an intramolecular H-bond (Chong et al., 2006). Furthermore, this effect is amplified when the glycerol backbone has the 1,2-*sn* configuration, when the distance between O-2′ and OH-2 is short (Mannock et al., 1992, 1994; Kuttenreich et al., 1993; Pascher et al., 1992; Turner et al., 1992).

The dimensions and stability of the L_β, L_α and nonlamellar phases are also affected by the same headgroup hydration properties. The instability of the headgroup/interfacial hydration evident in the 1,2-*sn*-β-D-GalDAGs at lower temperatures (Koberl et al., 1998; Tenchova et al., 1996) is an extreme example, where the hydration of all lamellar and nonlamellar phases at higher temperatures is inhibited, reducing their dimensions by reducing d_w and the radius of the water core, R_w (Seddon et al., 2003). The data presented here for the *rac*-β-D-Gal and β-D-GlcDAGs show a moderate form of that behaviour as a function of chain length in Fig. 7. The β-D-Gal headgroup remains hydrated in

the *rac*-β-D-GalDAGs, but both the L_β phase and the H_{II} phase *d*-spacings plateau at longer chain lengths, indicating a chain length dependent decrease in d_w and R_w at the phase transition. Nevertheless, the H_{II} phase *d*-spacings for the *rac*-β-D-GalDAG are higher than those of the *rac*-β-D-GlcDAGs, unlike their 1,2-*sn* counterparts. This observation suggests that when the *rac*-β-D-Gal headgroup is fully hydrated, it has a slightly greater hydrated volume than that of the *rac*-β-D-Glc headgroup. Together, these observations suggest that the 2,3-*sn*-glycerol configuration may be preferred in the extreme environments inhabited by halotolerant and methanogenic archaebacteria (Smith, 1988) because lipids with the 2,3-*sn* configuration are more likely to remain hydrated and, in doing so, to maintain membrane integrity.

The thermodynamic and structural measurements of the motionally averaged L_β and L_α phases for lipids with different headgroups (β-D-Gal, β-D-Glc, phosphorylethanolamine) behave in a similar manner, supporting the idea that the hydrocarbon chains determine the molecular area in the lamellar phase (Mannock et al., 2001a; Harper et al., 2001). However, in the nonlamellar phases, the GGLs and PEs exhibit a very different chain length-dependent change in H_{II} phase *d*-spacing, probably reflecting their differences in headgroup structure (ring versus chain), motion, hydration and the nature of the headgroup interactions (van der Waals forces and H-bonding interactions versus coulombic interactions). However, it is interesting that the PEs and GGLs have similar patterns of phase behaviour, despite their radically different headgroup interactions, and that while the lateral expansion of the hydrocarbon chains drives the formation of those nonlamellar phases, their geometry and phase dimensions are determined by the collective headgroup properties.

A simple thermodynamic and structural analysis of lipid lamellar and nonlamellar polymorphism continuing on from earlier work (Mannock et al., 2001a; Turner et al., 1992; Harper et al., 2001) will be presented in a forthcoming manuscript (Mannock et al., in preparation).

Note added in proof

A recent computer simulation of bilayers formed by alkyl glycosides has suggested that the structure and stability of the ordered phases in such compounds is determined by a balance between the inter- and intralamellar hydrogen bonds and that balance changes with the sugar stereochemistry and the orientation at the anomeric carbon atom (Chong et al., 2007).

Acknowledgements

This work was supported by operating and major equipment grants from the Medical Research Council of Canada (R.N.M.), by major equipment grants from the Alberta Heritage Foundation for Medical Research (R.N.M.), by National Institutes of Health grant GM32614 (S.M.G.) and Department of Energy grant DE-FG02-97ER62443 (S.M.G.). P.E.H. gratefully acknowledges fellowship assistance from the National Science Foundation and the Liposome Co.

References

Abrahamsson, S., Dahlen, B., Lofgren, H., Pascher, J., 1978. Lateral packing of hydrocarbon chains. Prog. Chem. Fats Other Lipids 16, 125–143.

Almond, A., 2005. Towards understanding the interaction between oligosaccharides and water molecules. Carbohyd. Res. 340, 907–920.

Asgharian, B., Cadenhead, D.A., Mannock, D.A., Lewis, R.N.A.H., McElhaney, R.N., 2000. A comparative monolayer film behavior study of monoglycosyl diacylglycerols containing linear, methyl and ϖ-cyclohexyl fatty acids. Langmuir 16, 7315–7317.

Baumann, W.J., Mangold, H.K., 1966a. Alkoxylipids. I. Preparation and characterization of alkoxy-diglycerides and dialkoxyglycerides. Biochim. Biophys. Acta 116, 570–576.

Baumann, W.J., Mangold, H.K., 1966b. Reactions of aliphatic methanesulfonates. II. Syntheses of long-chain di- and trialkyl glyceryl ethers. J. Org. Chem. 31, 498–500.

Benning, C., 1998. Biosynthesis and function of the sulfolipid sulfoquinovosyl diacylglycerol. Annu. Rev. Plant Physiol. Plant Mol. Biol. 49, 53–75.

Brain, P.M., Steers, T., Hui, S.W., Yeagle, P.L., Silvius, J.R., 1986. Role of head group structure in the phase behavior of amino phospholipids 2. Lamellar and nonlamellar phases of unsaturated phosphatidylethanolamine analogs. Biochemistry 25, 4259–4267.

Brennan, R.J., 1988. In: Ratledge, C., Wilkinson, S.G. (Eds.), Microbial Lipids, vol. 1. Academic Press, New York, pp. 202–299 (Chapter 6).

Broadhurst, M.G., 1962. An analysis of solid phase behaviour of normal paraffins. J. Res. Natl. Bur. Stand. Sect. A 66A, 241.

Brogi, A., Presentini, R., Moretti, E., Strazza, M., Piomboni, P., Costantino-Ceccarini, E., 1998. New insights into the interaction between the gpl20 and the HIV receptor in human sperm. J. Reprod. Immunol. 41, 213–231.

Bruzik, K.S., Tsai, M.D., 1987. A calorimetric study of the thermotropic behavior of pure sphingomyelin diastereomers. Biochemistry 26, 5364–5368.

Camara-Artigas, A., Brune, D., Allen, J.P., 2002. Interactions between lipids and bacterial reaction centers determined by protein crystallography. Proc. Natl. Acad. Sci. U.S.A. 99 (17), 11055–11060.

Chapman, D., 1965. The Structure of Lipids. John Wiley and Sons, NY (pp. 221–315, Chapter 8).

Cheetham, N.W.H., Lam, K., 1996. Molecular dynamics simulations of glycosides in aqueous solution. Carbohyd. Res. 282, 13–23.

Chevallier, V., Petitjean, D., Ruffier-Meray, V., Dirand, M., 1999. Correlations between the crystalline long *c*-parameter and the number of carbon atoms of pure n-alkanes. Polymer 40, 5953–5956.

Chong, T.T., Hashim, R., Bryce, R.A., 2006. Molecular dynamics simulation of monoalkyl glycoside micelles in aqueous solution: influence of carbohydrate headgroup stereochemistry. J. Phys. Chem. B 110, 4978–4984.

Chong, et al., 2007. Computer modelling and simulations of thermotropic and lyotropic alkyl glycoside bilayers. Liquid Crystals 34, 349–363.

Colombo, D., Compostella, F., Ronchetti, F., Reza-Elahi, S., Scala, A., Toma, L., et al., 2002. Inhibitory effect of stabilized analogues of glycoglycerolipids on Epstein-Barr virus activation and mouse skin tumor promotion. Cancer Lett. 186, 37–41.

Dashnau, J.L., Sharp, K.A., Vanderkooi, J.M., 2005. Carbohydrate intramolecular hydrogen bonding cooperativity and its effect on water structure. J. Phys. Chem. B 109, 24152–24159.

Di Gregorio, G.M., Mariani, P., 2005. Rigidity and spontaneous curvature of lipidic monolayers in the presence of trehalose: a measurement in the DOPE inverted hexagonal phase. Eur. Biophys. J. 34, 67–81.

Erbes, J., Czeslik, C., Hahn, W., Winter, R., Rappolt, M., Rapp, G., 1994. On the existence of bicontinuous cubic phases in dioleoylphosphatidylethanolamine. Ber. Buns. Phys. Chem. 98, 1287–1293.

Fabri, D., Williams, M.A.K., Halstead, T.K., 2005. Water T2 relaxation in sugar solutions. Carbohyd. Res. 340, 889–905.

Fang, H., Zhang, M., Shi, W.-H., Wan, T.-L., 2006. Facile synthesis of ordered large-pore mesoporous silica thin film with $Im\bar{3}m$ symmetry using n-butanol as the cosurfactant. J. Non-Cryst. Solids 352, 2279–2283.

Fischer, W., 1990. In: Kates, M. (Ed.), Glycolipids, Phosphoglycolipids and Sulfoglycolipids. Handbook of Lipid Research, vol. 6. Plenum Press, New York, pp. 123–234.

Gabke, A., Kraineva, J., Kohling, R., Winter, R., 2005. Using pressure in combination with X-ray and neutron scattering techniques for studying the structure, stability and phase behaviour of soft condensed matter and biomolecular systems. J. Phys. Condens. Matter 17, S3077–S3092.

Gadella, B., Lopes-Cardozo, M., van Golde, L., Colenbrander, B., Gadella, T., 1995. Glycolipid migration from the apical to the equatorial subdomains of the sperm head plasma membrane precedes the acrosome reaction. Evidence for a primary capacitation event in boar spermatozoa. J. Cell. Sci. 108, 935–946.

Galema, S.A., Hoiland, H., 1991. Stereochemical aspects of hydration of carbohydrates in aqueous solutions. 3. Density and ultrasound measurements. J. Phys. Chem. 95, 5321–5326.

Gruner, S.M., Milch, J.R., Reynolds, G.T., 1982. A slow scan SIT-TV detector for quantitative recording of weak X-ray diffraction images. Rev. Sci. Instrum. 53, 1770–1778.

Hagio, M., Gombos, Z., Varkonyi, Z., Masamoto, K., Sato, N., Tsuzuki, M., et al., 2000. Direct evidence for requirement of phosphatidylglycerol in photosystem II of photosynthesis. Plant Physiol. 124, 795–804.

Harper, P.E., Mannock, D.A., Lewis, R.N.A.H., McElhaney, R.N., Gruner, S.M., 2001. X-ray diffraction structures of some phosphatidylethanolamine lamellar and inverted hexagonal phases. Biophys. J. 81, 2693–2706.

Hartel, H., Essigmann, B., Lokstein, H., Hoffmann-Benning, S., Peters-Kottig, M., Benning, C., 1998. The phospholipid-deficient phol mutant of *Arabidopsis thaliana* is affected in the organization, but not in the light acclimation, of the thylakoid membrane. Biochim. Biophys. Acta 1415, 205–218.

Hauser, H., Pascher, I., Pearson, R.H., Sundell, S., 1981. Preferred conformation and molecular packing of phosphoethanolamine and phosphatidylcholine. Biochim. Biophys. Acta 650, 21–51.

Hinz, H.-J., Kuttenreich, H., Meyer, R., Renner, M., Frund, R., Koynova, R., Boyanova, A.I., Tenchov, B., 1991. Stereochemistry and size of sugar headgroups determine structure and phase behaviour of glycolipid membranes: densimetric, calorimetric and X-ray studies. Biochemistry 30, 5125–5138.

Honke, K., Hirahara, Y., Dupree, J., Suzuki, K., Popko, B., Fukushima, K., Fukushima, J., Nagasawa, T., et al., 2002. Paranodal junction formation and spermatogenesis require sulfoglycolipids. Proc. Natl. Assoc. Sci. U.S.A. 99, 4227–4232.

Ishizuka, I., Yamakawa, T., 1985. In: Wiegandt, H. (Ed.), Glycolipids. New Comprehensive Biochemistry, vol. 10. Elsevier Science, New York, pp. 101–198 (Chapter 2).

Jarrell, H.C., Wand, A.T., Giziewicz, J.B., Smith, I.C.P., 1987. The dependence of glyceroglycolipid orientation and dynamics on head-group structure. Biochim. Biophys. Acta 897, 69–82.

Khan, A., Rilfors, L., Wieslander, A., Lindblom, G., 1981. The effect of cholesterol on the phase-structure of glucolipids from *Acholeplasma laidlawii* membranes. Eur. J. Biochem. 16, 215–220.

Kirschner, K.N., Woods, R.J., 2001. Solvent interactions determine carbohydrate conformation. Proc. Natl. Acad. Sci U.S.A. 98, 10541–10545.

Kitamura, H., Ohta, A., Sekimoto, M., Sato, M., Iwakabe, K., Nakui, M., Yahata, T., Meng, H., et al., 2000. Alpha-galactosylceramide induces early B-cell activation through IL-4 production by NKT cells. Cell. Immunol. 199, 37–42.

Koberl, M., Hinz, H.J., Rapp, G., 1998. Temperature scanning simultaneous small- and wide-angle X-ray scattering studies on glycolipid vesicles: areas, expansion coefficients and hydration. Chem. Phys. Lipids 91, 13–37.

Koynova, R., Brankov, J., Tenchov, B., 1997. Modulation of lipid phase behavior by kosmotropic and chaotropic solutes. Experiment and thermodynamic theory. Eur. Biophys. J. 25, 261–274.

Kraineva, J., Narayanan, R.A., Kondrashkina, E., Thiyagarajan, P., Winter, R., 2005. Kinetics of lamellar-to-cubic and intercubic phase transitions of pure and cytochrome c containing monoolein dispersions monitored by time-resolved small-angle X-ray diffraction. Langmuir 21, 3559–3571.

Kuttenreich, H., Hinz, H.-J., Inczedy-Marcsek, M., Koynova, R., Tenchov, B., Laggner, P., 1988. Polymorphism of synthetic 1,2-*O*-dialkyl-3-*O*-β-D-galactosyl-*sn*-glycerols of different alkyl chain lengths. Chem. Phys. Lipids 47, 245–260.

Kuttenreich, H., Hinz, H.-J., Koynova, R.D., Tenchov, B.G., 1993. Different phase behavior of the *sn*-1 and *sn*-3 stereoisomers of the glycolipid di-tetradecyl-β-D-galactosylglycerol. Chem. Phys. Lipids 66, 55–62.

Lau, A.F., Siedlecki, J., Anleitner, J., Patterson, G.M.L., Caplan, F.R., Moore, R.E., 1993. Inhibition of reverse transcriptase activity by extracts of cultured blue-green algae (Cyanophyta). Planta Med. 59, 101–194.

Lewis, R.N.A.H., Mannock, D.A., McElhaney, R.N., 1997. Membrane lipid molecular structure and polymorphism. In: Epand, R. (Ed.), Lipid Polymorphism and Membrane Properties. Current Topics in Membranes, vol. 44. Academic Press, pp. 25–102.

Li, H.-W., Strauss, H.L., Snyder, R.G., 2004. Differences in the IR methylene rocking bands between the crystalline fatty acids and *n*-alkanes: frequencies, intensities, and correlation splitting. J. Phys. Chem. A 108, 6629–6642.

Lingwood, C., Schramayr, S., Quinn, P., 1990. Male cell specific sulfogalactoglycero-lipid is recognized and degraded by mycoplasmas associated with male infertility. J. Cell Physiol. 142, 170–176.

Lis, L.J., Quinn, P.J., 1986. A time-resolved synchrotron X-ray study of a crystalline phase bilayer transition and packing in a saturated monogalactosyldiacylglycerol-water system. Biochim. Biophys. Acta 862, 81–86.

Loya, S., Reshef, V., Mizrachi, E., Silberstein, C., Rachamim, Y., Carmeli, S., et al., 1998. The inhibition of the reverse transcriptase of HIV-1 by the natural sulfoglycolipids from cyanobacteria: contribution of different moieties to their high potency. J. Natl. Prod. 61, 891–895.

Lu, X., Rengan, K., Bittman, R., Arthur, G., 1994. The α- and β-anomers of 1-*O*-hexadecyl-2-*O*-methyl-3-*S*-thioglucosyl-*sn*-glycerol inhibit the proliferation of epithelial cancer cell lines. Oncol. Rep. 1, 933–936.

Luzzati, V., 1968. In: Chapman, D. (Ed.), Biological Membranes, Physical Fact and Function. Academic Press, NY, pp. 71–123 (see p. 118–119).

Mannock, D.A., McElhaney, R.N., 1991. Differential scanning calorimetry and X-ray diffraction studies of a series of synthetic β-D-galactosyl diacylglycerols. Biochem. Cell Biol. 69, 863–867.

Mannock, D.A., McElhaney, R.N., 2004. Thermotropic and lyotropic phase properties of glycolipid diastereomers: role of headgroup and interfacial interactions in determining phase behaviour. Curr. Opin. Colloid Interface Sci. 8, 426–444.

Mannock, D.A., Brain, A.P.R., Williams, W.P., 1985a. The phase behavior of 1,2-diacyl-3-monogalactosyl-*sn*-glycerol derivatives. Biochim. Biophys. Acta 817, 289–298.

Mannock, D.A., Brain, A.P.R., Williams, W.P., 1985b. Phase behaviour of the membrane lipids of the thermophilic blue-green-alga, *Anacystis nidulans*. Biochim. Biophys. Acta 821, 153–164.

Mannock, D.A., Lewis, R.N.A.H., McElhaney, R.N., 1987. An improved procedure for the preparation of 1,2-di-*O*-acyl-3-*O*-(β-D-glucopyranosyl)-*sn*-glycerols. Chem. Phys. Lipids 43, 113–127.

Mannock, D.A., Lewis, R.N.A.H., McElhaney, R.N., Akiyama, M., Yamada, H., Turner, D.C., Gruner, S.M., 1992. Effect of the chirality of the glycerol backbone on the bilayer and nonbilayer phase-transitions in the diastereomers of di-dodecyl-β-D-glucopyranosyl-glycerol. Biophys. J. 63, 1355–1368.

Mannock, D.A., McElhaney, R.N., Harper, P.E., Gruner, S.M., 1994. Differential scanning calorimetry and X-ray-diffraction studies of the thermotropic phase behavior of the diastereomeric di-tetradecyl-β-D-galactosyl-glycerols and their mixture. Biophys. J. 66, 734–740.

Mannock, D.A., Akiyama, M., Lewis, R.N.A.H., McElhaney, R.N., 2000. Synthesis and thermotropic characterization of a homologous series of racemic β-D-glucosyl dialkylglycerols. Biochim. Biophys. Acta 1509, 203–215.

Mannock, D.A., Lewis, R.N.A.H., McElhaney, R.N., Harper, P.E., Gruner, S.M., 2001a. Relationship between fatty acid composition and the lamellar gel to liquid crystalline and the lamellar to inverted non-lamellar phase transition temperatures of phosphatidylethanolamines and diacyl-α-D-glucosyl-glycerols. Eur. Biophys. J. 30, 537–554.

Mannock, D.A., Harper, P.E., Gruner, S.M., McElhaney, R.N., 2001b. The physical properties of glycosyl diacylglycerols. Calorimetric, X-ray diffraction and Fourier transform spectroscopic studies of a homologous series of 1,2-di-O-acyl-3-*O*-(β-D-galactopyranosyl)-*sn*-glycerols. Chem. Phys. Lipids 111, 139–161.

Mason, P.E., Neilson, G.W., Enderby, J.E., Saboungi, M.-L., Brady, J.W., 2005. Structure of aqueous glucose solutions as determined by neutron diffraction with isotopic substitution experiments and molecular dynamics calculations. J. Phys. Chem. B 109, 13104–13111.

Minoda, A., Sato, N., Nozaki, H., Okada, K., Takahashi, H., Sonoike, K., et al., 2002. Role of sulfoquinovosyl diacylglycerol for the maintenance of photosystem II in *Chlamydomonas reinhardtii*. Eur. J. Biochem. 269, 2353–2358 (Erratum in: Eur. J. Biochem. 269 (12) 3093).

Mizushina, Y., Xu, X., Asahara, H., Takeuchi, R., Oshige, M., Shimazaki, N., et al., 2003. A sulfoquinovosyl diacylglycerol is a DNA polymerase epsilon inhibitor. Biochem. J. 370, 299–305.

Murakami, C., Yamazaki, T., Hanashima, S., Takahashi, S., Takemura, M., Yoshida, S., et al., 2003. A novel DNA polymerase inhibitor and a potent apoptosis inducer: 2-mono-*O*-acyl-3-*O*-(α-D-sulfoquinovosyl)-glyceride with stearic acid. Biochim. Biophys. Acta Proteins Proteomics 1645, 72–80.

Nakaoki, T., Nagano, H., Yanagida, T., 2004. Molecular mobility depending on chain length and thermally induced molecular motion of n-alkane/urea inclusion compounds. J. Mol. Struct. 699, 1–7.

Nakata, K., Guo, C.T., Matsufuji, M., Yoshimoto, A., Inagaki, M., Higuchi, R., Suzuki, Y., 2000. Influenza A virus-binding activity of glycoglycerolipids of aquatic bacteria. J. Biochem. 127, 191–198.

Nicol, A., Nieda, M., Koezuka, Y., Porcelli, S., Suzuki, K., Tadokoro, K., Durrant, S., Juji, T., 2000. Human invariant V alpha 24+ natural killer T cells activated by alpha-galactosylceramide (KRN7000) have cytotoxic anti-tumour activity through mechanisms distinct from T cells and natural killer cells. Immunology 99, 229–234.

Ogawa, T., Beppu, K., 1982. Synthetic studies on cell-surface glycans. 14. Synthesis of 3-*O*-glycosyl-1,2-di-*O*-tetradecyl-*sn*-glycerol. Agric. Biol. Chem. 46, 255–262.

Ohta, K., Mizushina, Y., Yamazaki, T., Hanashima, S., Sugawara, F., 2001. Specific interaction between an oligosaccharide on the tumor cell surface and the novel antitumor agents sulfoquinovosylacylglycerols. Biochem. Biophys. Res. Commun. 288, 893–900.

Oldani, D., Hauser, H., Nichols, B.W., Phillips, M.C., 1975. Monolayer characteristics of some glycolipids at air–water interface. Biochim. Biophys. Acta 382, 1–9.

Pascher, I., Lundmark, M., Nyholm, P.G., Sundell, S., 1992. Crystal structures of membrane lipids. Biochim. Biophys. Acta 1113, 339–373.

Pick, U., Weiss, M., Gounaris, K., Barber, J., 1987. The role of different thylakoid glycolipids in the function of reconstituted chloroplast ATP synthase. Biochim. Biophys. Acta 891, 28–39.

Quinn, P.J., Lis, L.J., 1987. Structural intermediates in phase-transitions involving crystalline phase bilayers of monogalactosyldiacylglycerol in water. J. Colloid Interface Sci. 115, 220–224.

Rappolt, M., Di Gregorio, G.M., Almgren, M., Amenitsch, H., Pabst, G., Laggner, P., Mariani, P., 2006. Non-equilibrium formation of the cubic $Pn\bar{3}\bar{m}$ phase in a monoolein/water system. Europhys. Lett. 75, 267–273.

Rivas, E., Luzzati, V., 1969. Polymorphism of polar lipids and galactolipids in maize chloroplasts in presence of water. J. Mol. Biol. 41, 261–275.

Sahara, H., Hanashima, S., Yamazaki, T., Takahashi, S., Sugawara, F., Ohtani, S., et al., 2002. Anti-tumor effect of chemically synthesized sulfolipids based on sea urchin's natural sulfonoquinovosylmonoacylglycerols. Jpn. J. Cancer Res. 93, 85–92.

Sanderson, P.W., Williams, W.P., 1992. Low temperature phase behavior of the major plant leaf lipid monogalactosyldiacylglycerol. Biochim. Biophys. Acta 1107, 77–85.

Sato, N., Sonoike, K., Tsuzuki, M., Kawaguchi, A., 1995. Impaired photosystem II in a mutant of *Chlamydomonas reinhardtii* defective in sulfoquinovosyl diacylglycerol. Eur. J. Biochem. 234, 16–23.

Sato, N., Aoki, M., Mara, Y., Sonoike, K., Minoda, A., Tsuzuki, M., 2003. Involvement of sulfoquinovosyl diacylglycerol in the structural integrity and heat-tolerance of photosystem II. Planta 217, 245–251.

Saubermann, L.J., Beck, P., De Jong, Y.P., Pitman, R.S., Ryan, M.S., Kim, H.S., Exley, M., et al., 2000. Activation of natural killer T cells by alpha-galactosylceramide in the presence of CDld provides protection against colitis in mice. Gastroenterology 119, 119–128.

Seddon, J.M., Cevc, G., Kaye, R.D., Marsh, D., 1984. X-ray diffraction study of the polymorphism of hydrated diacyl and dialkylphosphatidylethanolamines. Biochemistry 23, 2634–2644.

Seddon, J.M., Zeb, N., Templer, R.H., McElhaney, R.N., Mannock, D.A., 1996. An *Fd3m* lyotropic cubic phase in a binary glycolipid/water system. Langmuir 12, 5250–5253.

Seddon, J.M., Robins, J., Gulik-Krzywicki, T., Delacroix, H., 2000. Inverse micellar phases of phospholipids and glycolipids. Phys. Chem. Chem. Phys. 2, 4485–4493.

Seddon, J.M., Ces, O., Templer, R.H., Mannock, D.A., McElhaney, R.N., 2003. Structure and phase behaviour of synthetic glycolipids. Mol. Cryst. Liq. Cryst. 402, 77–84.

Sen, A., Mannock, D.A., Collins, D.J., Quinn, P.J., Williams, W.P., 1983. Thermotropic phase properties and structure of 1,2-distearoylgalactosylglycerols in aqueous systems. Proc. R. Soc. Lond. B218, 349–364.

Sen, A., Hui, S.-W., Mannock, D.A., Lewis, R.N.A.H., McElhaney, R.N., 1990. Physical properties of glycosyl diacylglycerols. 2. X-ray diffraction studies of a homologous series of 1,2-Di-O-acyl-3-*O*-(α-D-glucopyranosyl)-*sn*-glycerols. Biochemistry 29, 7799–7804.

Shipley, G.G., Green, J.P., Nichols, B.D., 1973. Phase behavior of monogalactosyl, digalactosyl, and sulfoquinovosyl diglycerides. Biochim. Biophys. Acta 311, 531–544.

Shyamsunder, E., Gruner, S.M., Tate, M.W., Turner, D.C., So, P.T.C., Tilcock, C.P.S., 1988. Observation of inverted cubic phase in hydrated dioleoylphosphatidylethanolamine membranes. Biochemistry 27, 2332–2336.

Silvius, J.R., Mak, N., McElhaney, R.N., 1980. Lipid and protein-composition and thermotropic lipid phase transitions in fatty acid homogeneous membranes of *Acholeplasma laidlawii* B. Biochim. Biophys. Acta 597, 199–215.

Silvius, J.R., Brain, P.M., O'Leary, T.J., 1986. Role of head group structure in the phase behavior of amino phospholipids 1. Hydrated and dehydrated lamellar phases of saturated phosphatidylethanolamine analogs. Biochemistry 25, 4249–4258.

Smith, P.F., 1988. In: Ratledge, C., Wilkinson, S.G. (Eds.), Microbial Lipids, vol. 1. Academic Press, New York, pp. 489–554 (Chapter 8).

Tate, M.W., Gruner, S.M., Eikenberry, E.F., 1997. Coupling format variations in X-ray detectors based on charge coupled devices. Rev. Sci. Instrum. 68, 47–54.

Tenchov, B., Koynova, R., Rappolt, M., Rapp, G., 1999. An ordered metastable phase in hydrated phosphatidylethanolamine: the Y-transition. Biochim. Biophys. Acta 1417, 183–190.

Tenchova, R., Tenchov, B., Hinz, H.J., Quinn, P.J., 1996. Lamellar non-lamellar phase transitions in synthetic glycoglycerolipids studied by time-resolved X-ray diffraction. Liq. Cryst. 20, 469–482.

Tristram-Nagle, S., Zhang, R., Suter, R.M., Worthington, C.R., Sun, W.-J., Nagle, J.F., 1993. Measurement of chain tilt angle in fully hydrated bilayers of gel phase lecithins. Biophys. J. 64, 1097–1109.

Trouard, T.P., Mannock, D.A., Lindblom, G., Rilfors, L., Akiyama, M., McElhaney, R.N., 1994. Thermotropic phase properties of 1,2-di-*O*-tetradecyl-(3-*O*-methyl-β-D-glucopyranosyl)-*sn*-glycerol. Biophys. J. 67, 1090–1100.

Tsuji, Y., Fukuda, H., Iuchi, A., Ishizuka, I., Isojima, S., 1992. Sperm immobilizing antibodies react to the 3-*O*-sulfogalactosyl residue of seminolipid on human sperm. J. Reprod. Immunol. 22, 225–236.

Turner, D.C., Gruner, S.G., Wang, Z.-G., Mannock, D.A., McElhaney, R.N., 1992. Structural study of the inverted cubic phases of di-dodecyl-β-D-glucopyranosyl-*rac*- glycerol. J. Physique II 2, 2039–2063.

White, D., Weerachatyanukul, W., Gadella, B., Kamolvarin, N., Attar, M., Tanphaichitr, N., 2000. Role of sperm sulfogalactosylglycerolipid in mouse sperm-zona pellucida binding. Biol. Reprod. 63, 147–155.

Wieslander, A., Ulmius, J., Lindblom, G., Fontell, K., 1978. Water binding and phase structures for different *Acholeplasma laidlawii* membrane lipids studies by deuteron nuclear magnetic-resonance and X-ray-diffraction. Biochim. Biophys. Acta 512, 241–253.

Wieslander, A., Rilfors, L., Johansson, L.B.-A., Lindblom, G., 1981a. Reversed cubic phase with membrane glucolipids from *Acholeplasma laidlawii*—H-1, H-2, and diffusion nuclear magnetic-resonance measurements. Biochemistry 20, 730–735.

Wieslander, A., Christiansson, A., Rilfors, L., Khan, A., Johansson, L.B.-A., Lindblom, G., 1981b. Lipid phase-structure governs the regulation of lipid-composition in membranes of *Acholeplasma laidlawii*. FEBS Lett. 124, 273–278.

Williams, W.P., Quinn, P.J., 1987. The phase behaviour of lipids in photosynthetic membranes. J. Bioenerg. Biomemb. 19, 605–624.

Wisner, D.A., Rosarro-Jansen, T., Tsai, M.D., 1986. Phospholipids chiral at phosphorus 12. Configurational effect on the thermotropic properties of chiral dipalmitoylthiophosphatidylcholine. J. Am. Chem. Soc. 108, 8064–8068.

Yang, L., Huang, H.W., 2003. A rhombohedral phase of lipid containing a membrane fusion intermediate structure. Biophys. J. 84, 1808–1817.

Yu, B., Xu, C., Benning, C., 2002. *Arabidopsis* disrupted in SQD2 encoding sulfolipid synthase is impaired in phosphate-limited growth. Proc. Natl. Acad. Sci. U.S.A. 99, 5732–5737.

Yue, A.W.B., Wong, B.C.-M., Rieder, J., Lewis, R.N.A.H., Mannock, D.A., McElhaney, R.N., 2003. The effect of independent variations in fatty acid structure and chain length on lipid polar headgroup composition in *Acholeplasma laidlawii* B membranes: regulation of lamellar/non-lamellar phase propensity. Biochemistry 42, 1309–1317.

Zhao, X., Wakamatsu, Y., Shibahara, M., Nomura, N., Geltinger, C., Nakahara, T., Murata, T., Yokoyama, K.K., 1999. Mannosylerythritol lipid is a potent inducer of apoptosis and differentiation of mouse melanoma cells in culture. Cancer Res. 59, 482–486.